Sources in CMB maps

Gianfranco De Zotti

INAF- Osservatorio Astronomico di Padova &
SISSA, Trieste

thanks to: Zhen-Yi Cai, Guillaume Castex and
Mattia Negrello

Point sources at 30, 143 and 857 GHz

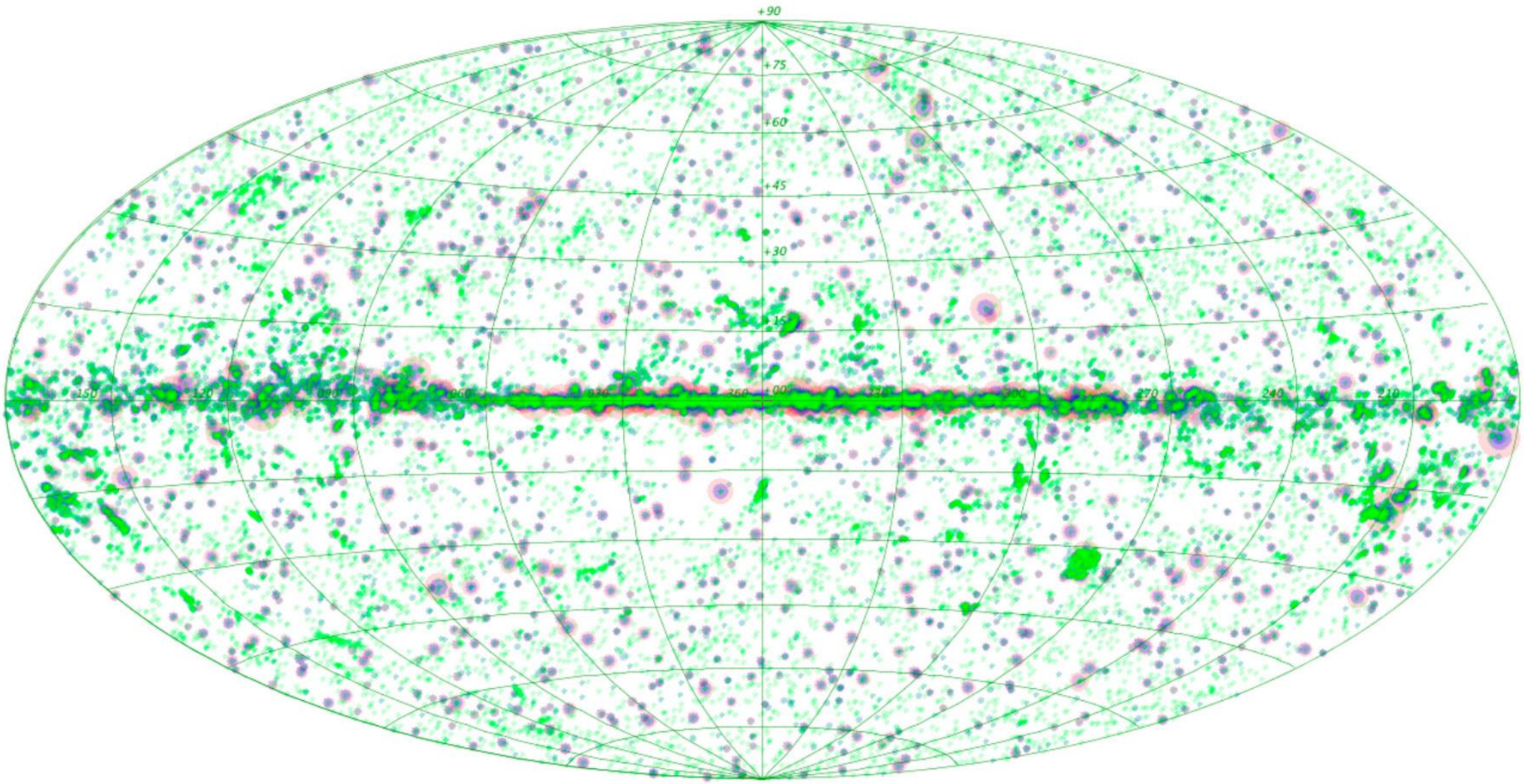

Sky distribution of the PCCS sources at three channels: 30 GHz (pink circles); 143 GHz (magenta circles); and 857 GHz (green circles). Planck Collaboration XXVIII (2013)

Radio sources vs dusty galaxies

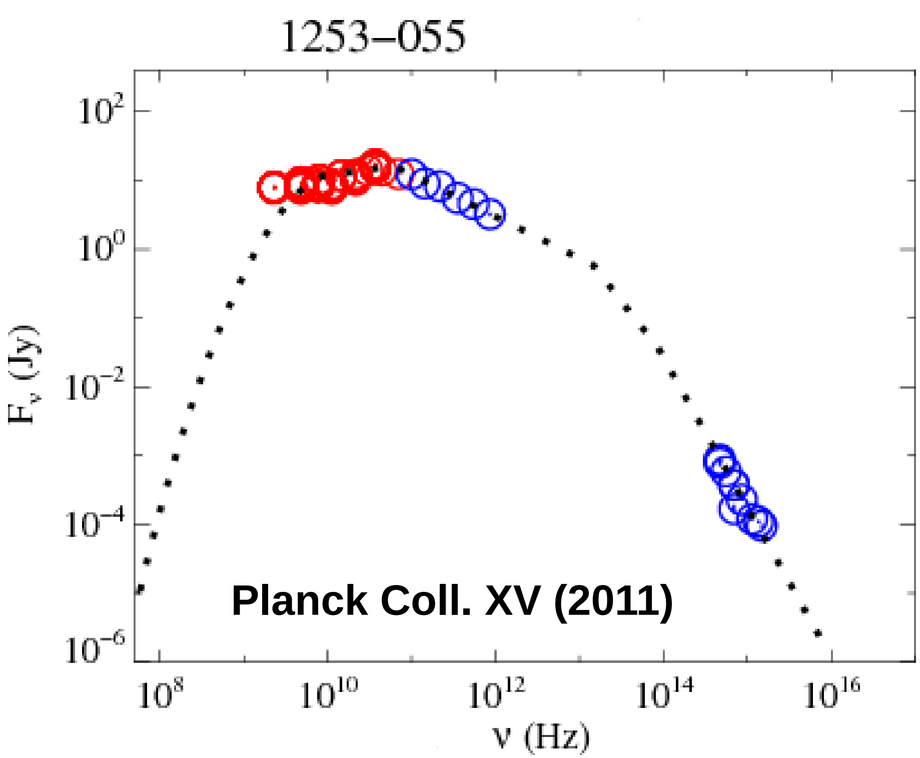

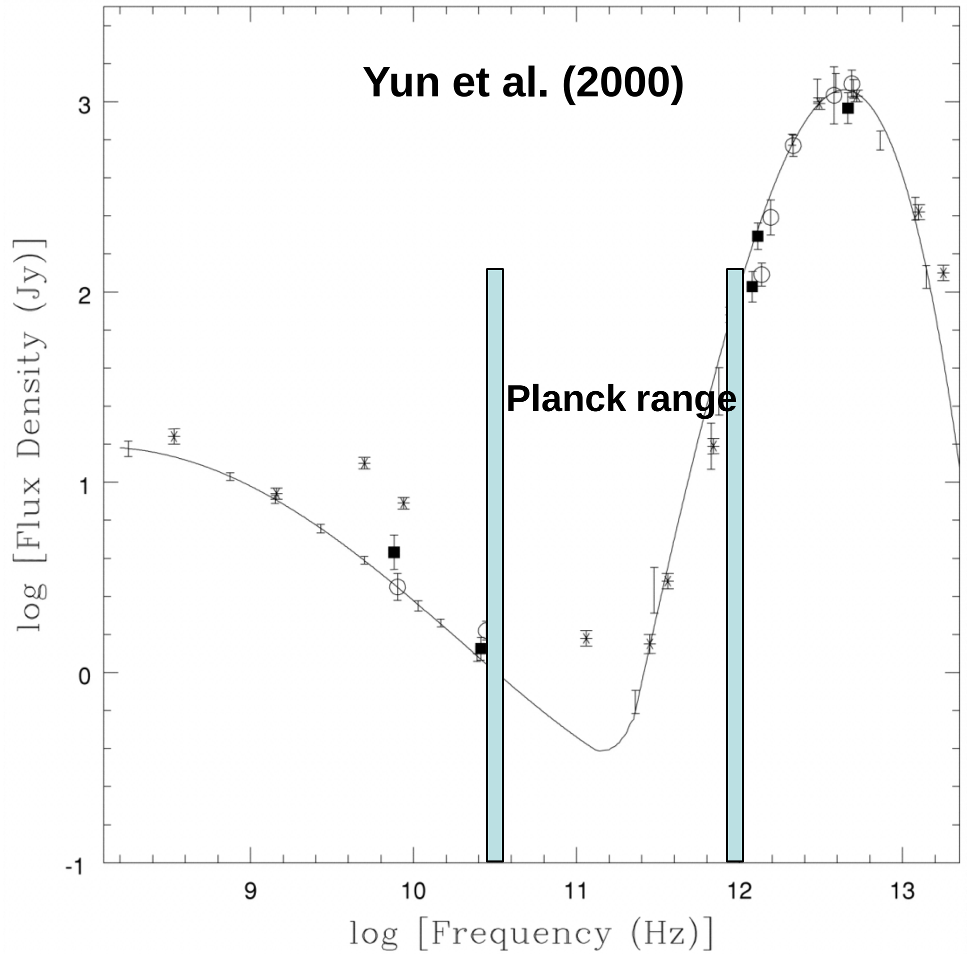

Red circles: LF data simultaneous to *Planck*; blue circles, Planck data and HF data simultaneous to *Planck*.

SEDs of 2 dusty QSOs (*squares* and *circles*) compared with that of the starburst galaxy M82. The y-scale is set for the flux density of M82.

Detection limits in CMB maps - 1

- In spite of the very high sensitivity of modern CMB experiments, they only provide *shallow* surveys of extragalactic sources.
- For example, the Planck 90% completeness limits of the Planck Catalogue of Compact Sources (PCCS) at 70, 100, 217 and 545 GHz are 776, 300,180 and 570 mJy (Planck 2013 XXVIII).
- For comparison, the 5σ instrumental noise limits at the same frequencies are ~255, 50, 45, and 165 mJy, respectively (Mennella et al. 2011; Planck HFI Core Team 2011).

Detection limits in CMB maps - 2

- This means that the surveys are limited by fluctuations of sky signals, not by instrumental noise: there is a lot of useful information in the fluctuation field!
- A further cue comes considering the number of detections per resolution element. For example, the PCCS has 332, 845, 1901 and 3738 detections at 70, 100, 217 and 545 GHz, respectively, above the 90% completeness level in the extragalactic zone. This means that there are 2143, 1599, 2658 and 1537 resolution elements/source, well above the values (30-40 resolution elements/source) usually assumed to correspond to the source confusion limit.

Fluctuation amplitude vs FWHM

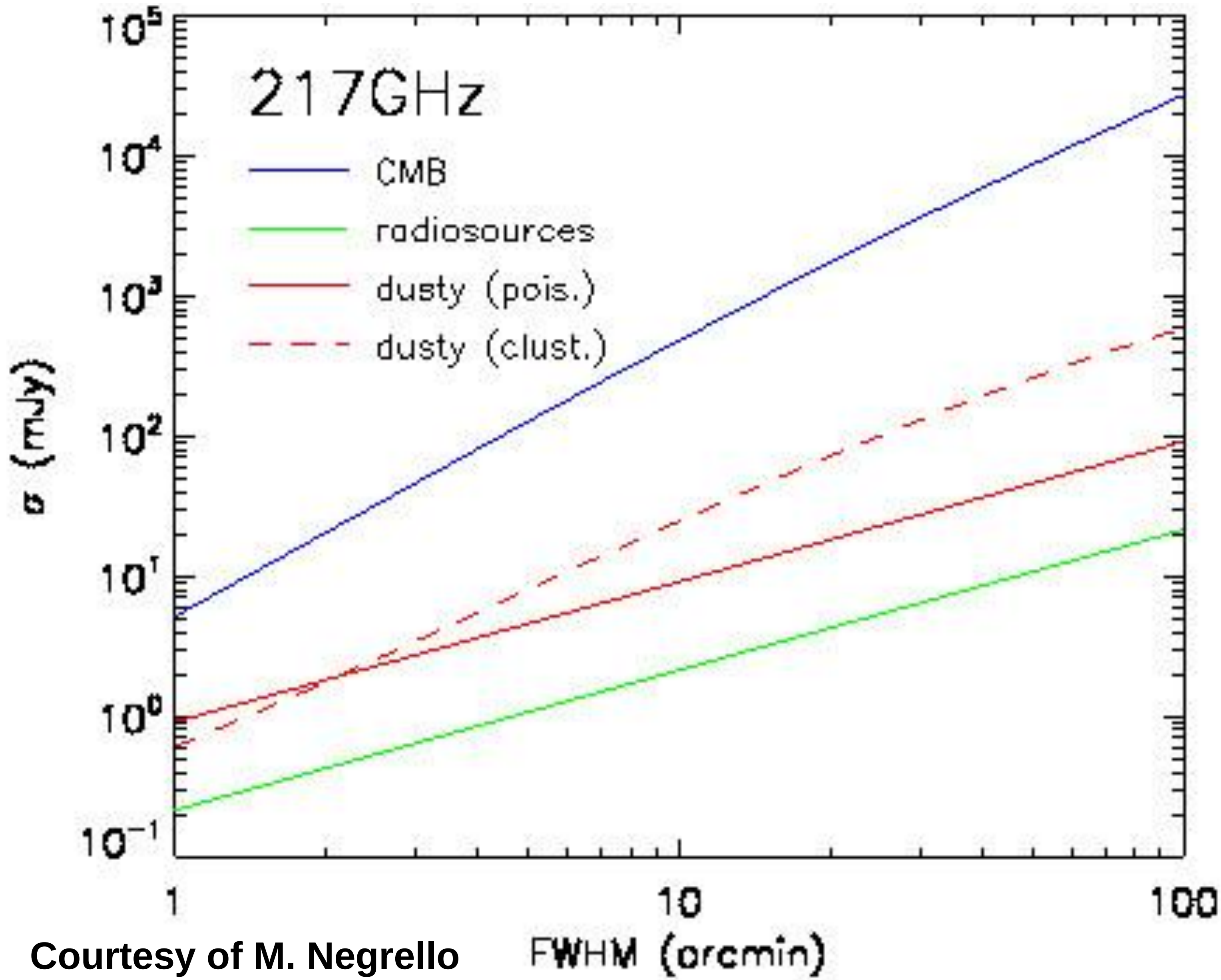

Courtesy of M. Negrello

Fluctuation amplitude vs frequency for diffraction limited measurements

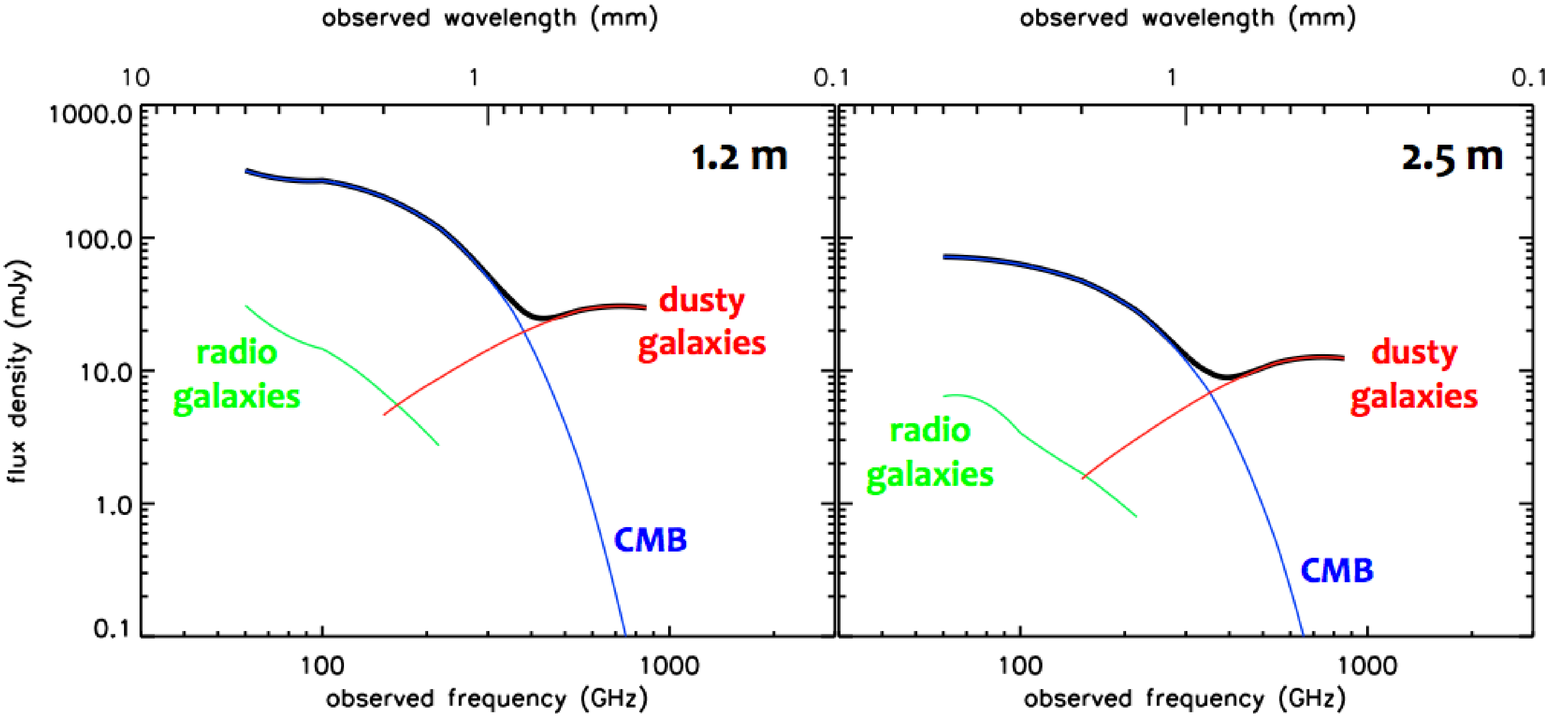

Courtesy of M. Negrello

Radio sources - 1

- A lot of results on radio sources presented in Planck Early Papers (Planck early results. XIII, XIV, XV).
- Major result: realization that for blazars (flat-spectrum radio quasars - FSRQs - and BL Lacs) already a ~ 70 GHz we are observing a downwards bending of the spectra.
- Result unexpected in the framework of the `blazar sequence' model according to which the peak frequency is anticorrelated with radio luminosity and occurs in the millimetric region only for the rare exceptionally luminous objects, not for the general population.
- Interesting implications for the blazar physics (Tucci et al. 2011)

Planck radio-source counts -1

(Planck Collaboration XIII 2011)

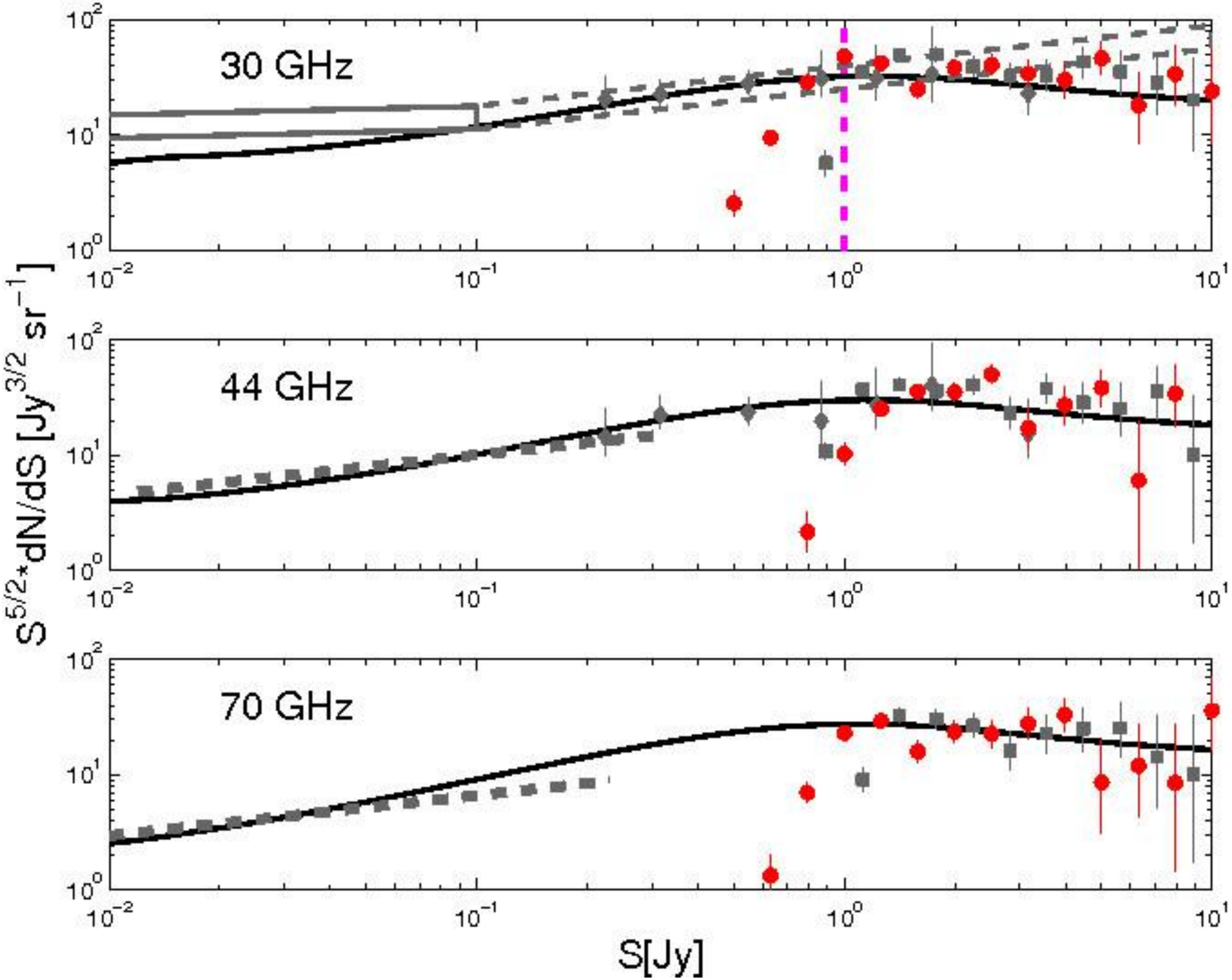

Grey squares: WMAP; grey diamonds: extrap. from 20 GHz; boxes: DASI (dashed) and VSA (solid) Dashed lines: extrapolations from 15 GHz

Planck radio-source counts - 2

(Planck Collaboration XIII 2011)

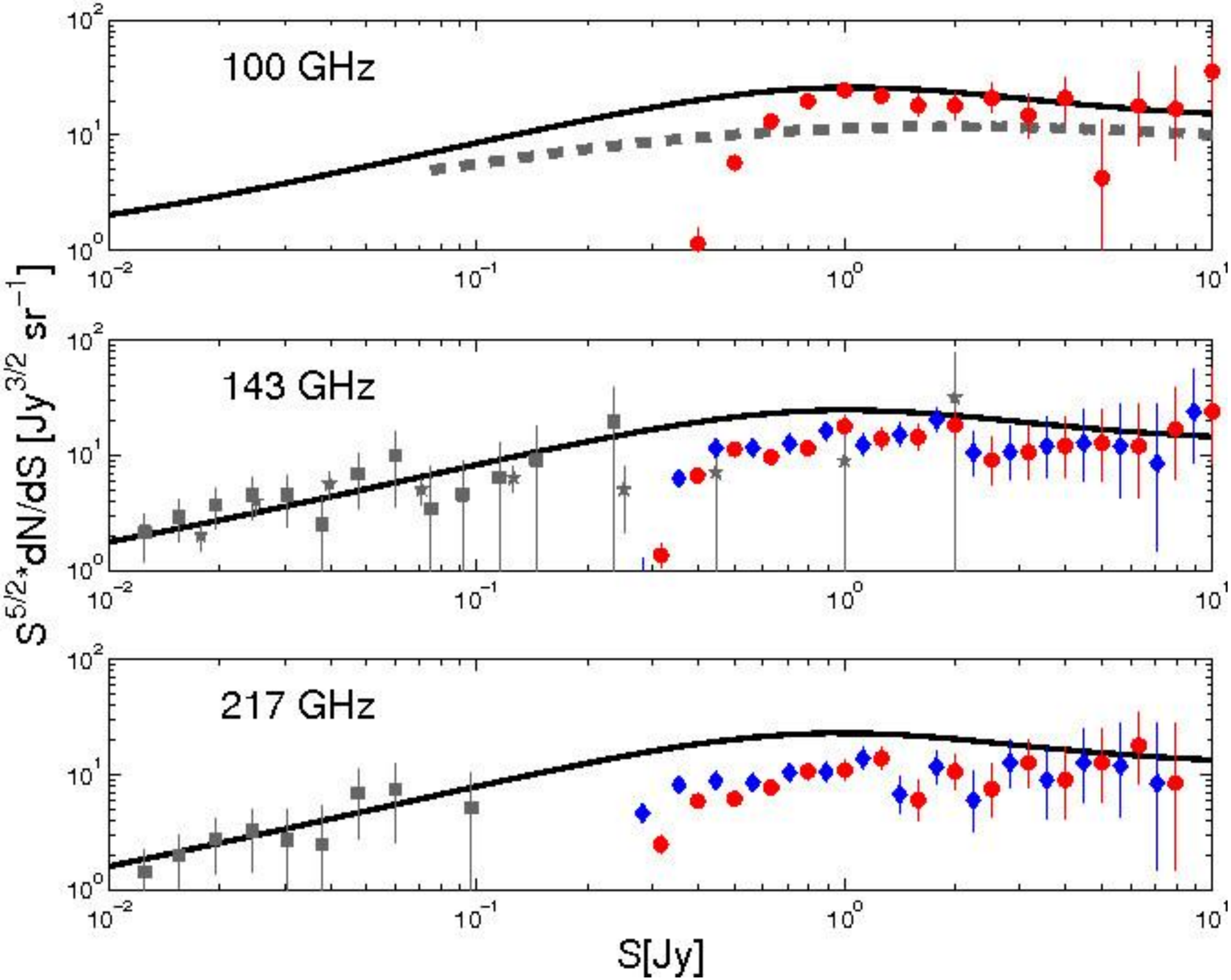

Dashed line: extrapolation from 15 GHz.

Grey squares: SPT counts

Planck radio-source counts - 3

(Planck Collaboration XIII 2011)

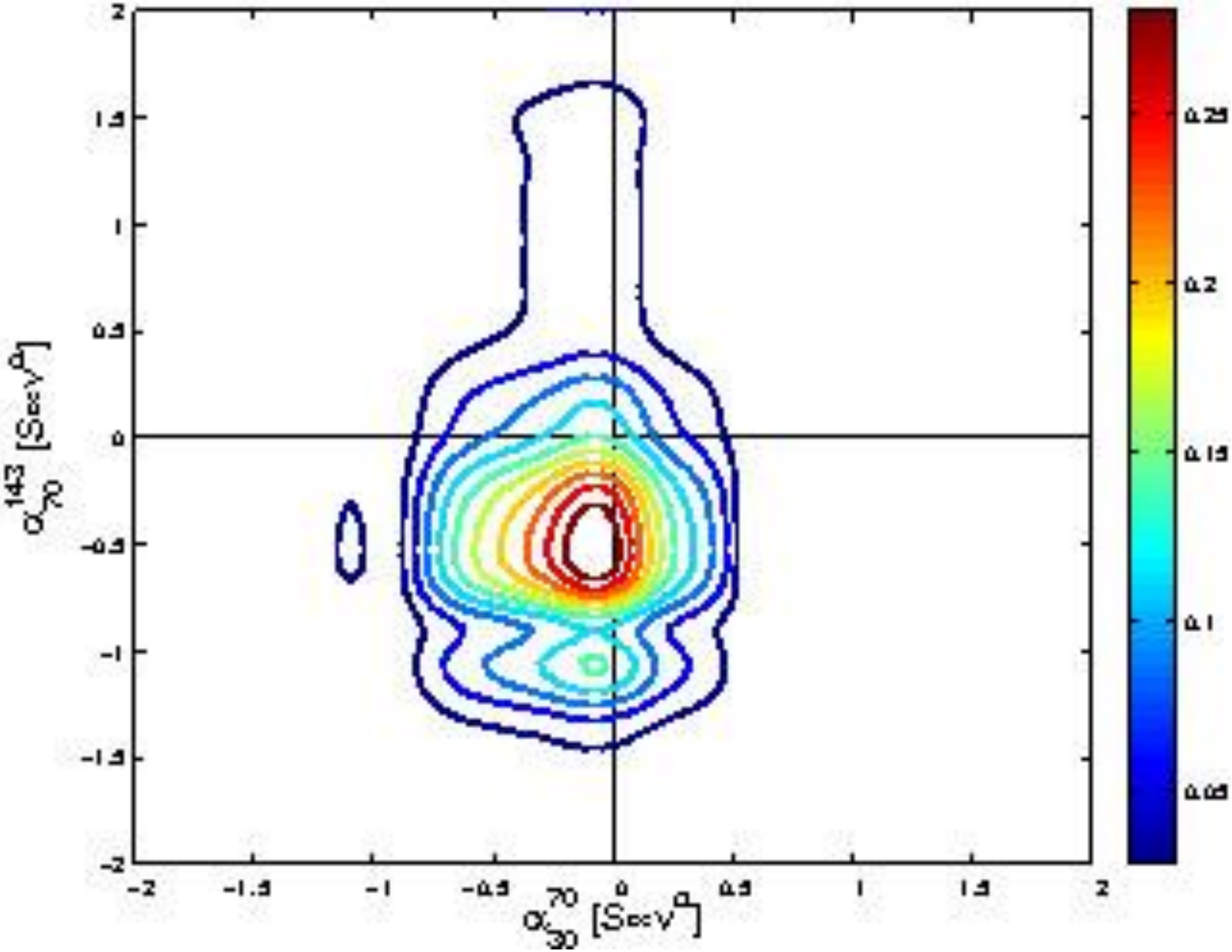

Contour levels of 143-70 GHz vs 70-30 GHz spectral indices. The maximum probability corresponds to $\alpha^{143}{}_{70}$ = -0.50 and $\alpha^{70}{}_{30}$ = -.18

Counts and break frequencies

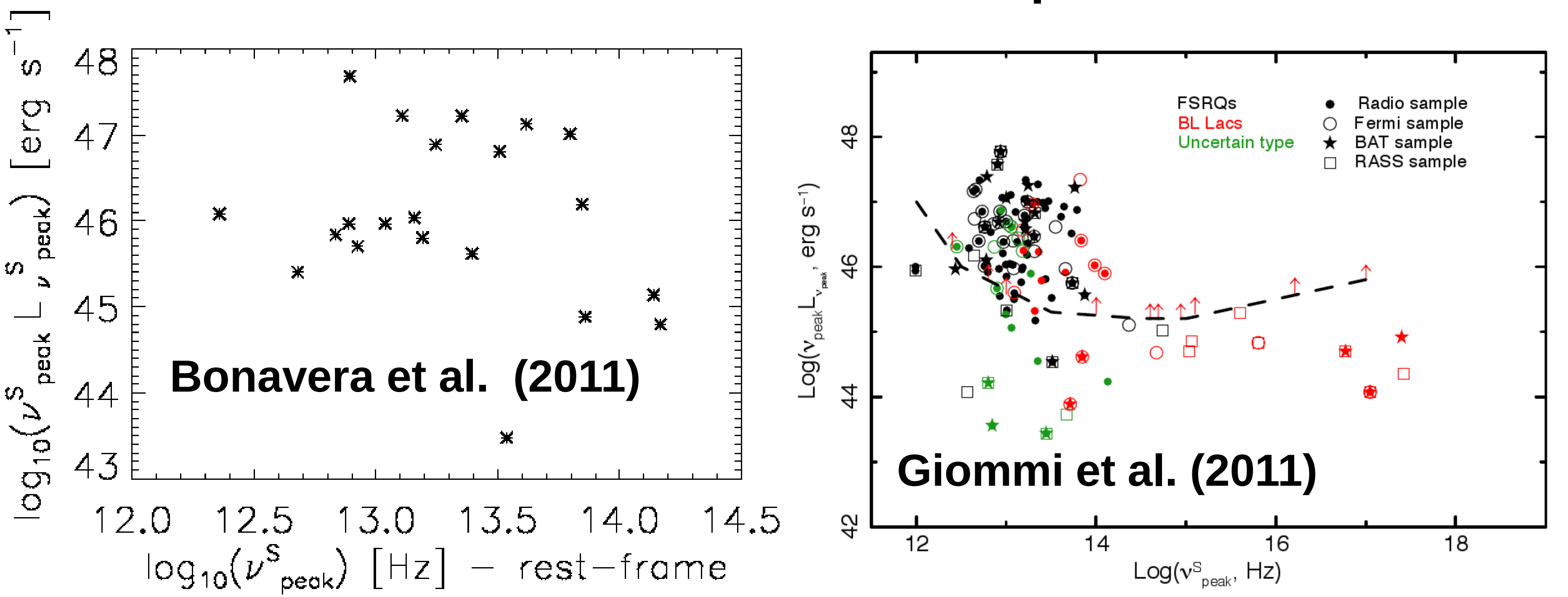

Contrary to expectations from the blazar sequence model, there is no correlation between luminosity and peak frequency. BL Lacs found to have higher break frequencies compared to FSRQs (Massardi et al. 2011; Bonavera et al. 2011; Richards et al. 2011; Planck early results. XIV, XV; Giommi et al. 2011). Above the dashed line in the right-hand panel, the non-thermal optical light of blazars is bright enough to swamp the emission from the host galaxy.

Spectral Energy Distributions

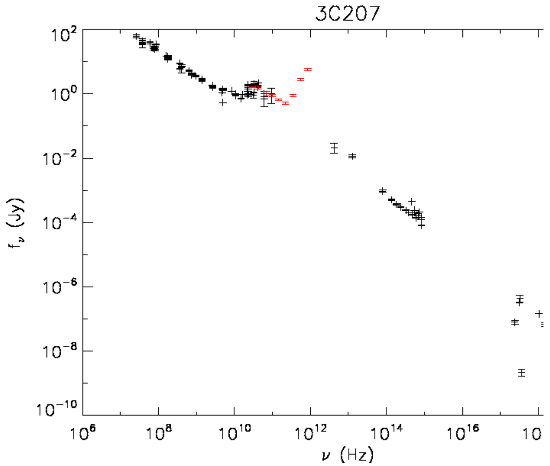

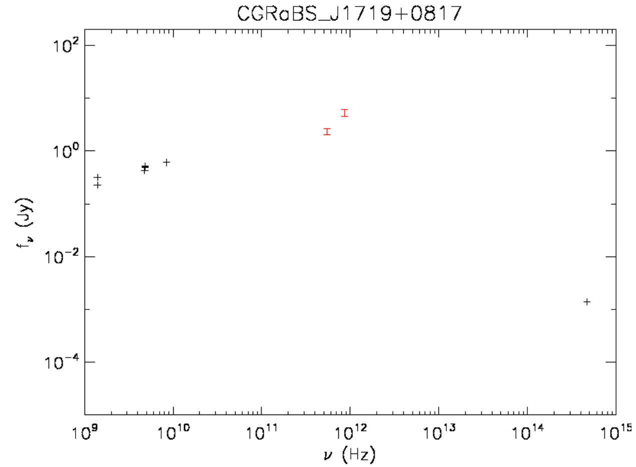

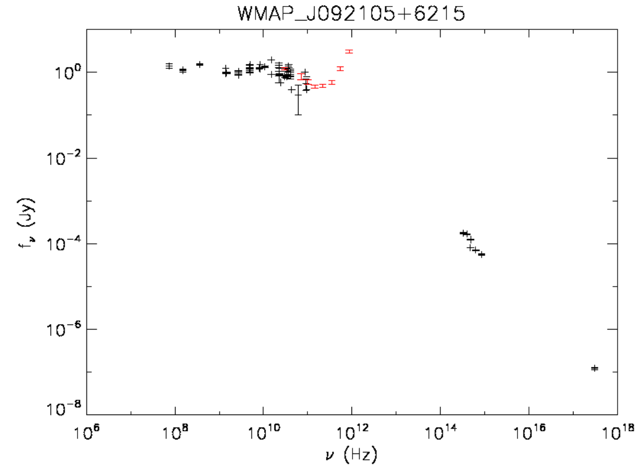

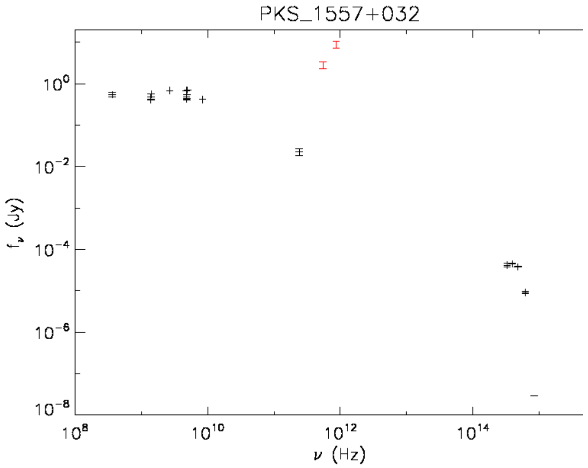

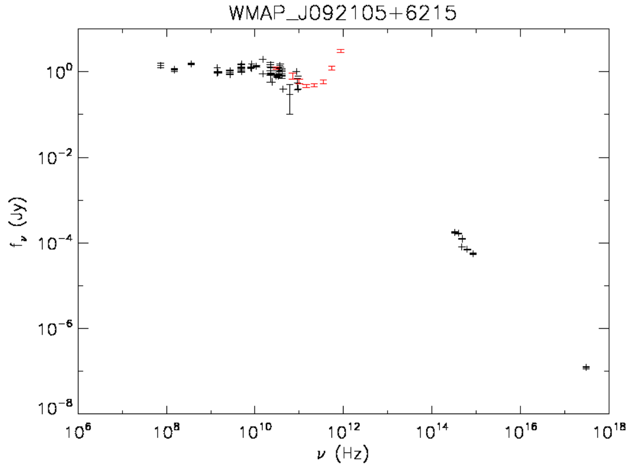

The sub-mm flux density of 5 (+1?) out of 12 (+1?) BZCAT blazars listed in the Planck ERCSC 857 GHz catalog is dominated by thermal dust emission.

May be lost by colour selection; synchrotron/dust emission at transition frequencies may be overestimated. **Courtesy of M. Clemens**

Dusty galaxies

Most Planck high-|b| sub-mm sources are local galaxies

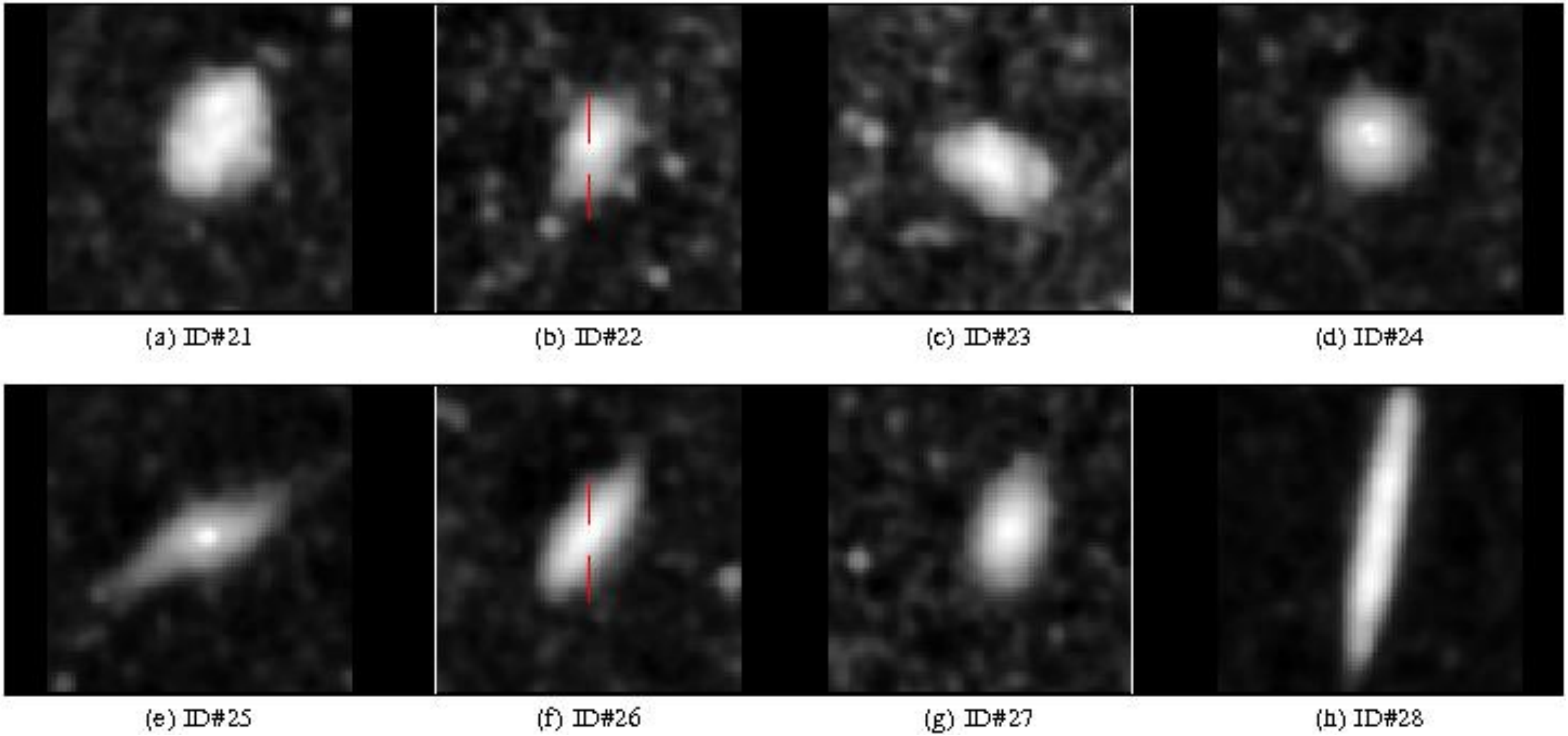

Herschel-SPIRE images of some Planck-ERCSC sources in the H-ATLAS GAMA 9h field (Herranz et al. 2013)

Counts and local luminosity functions of dusty galaxies

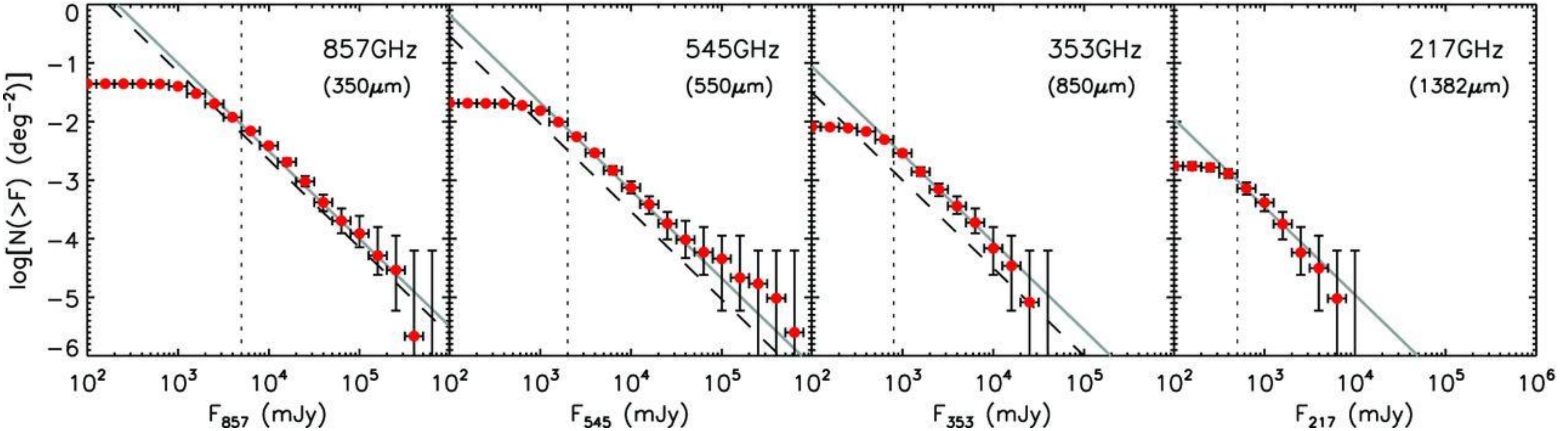

Negrello et al. (2013)

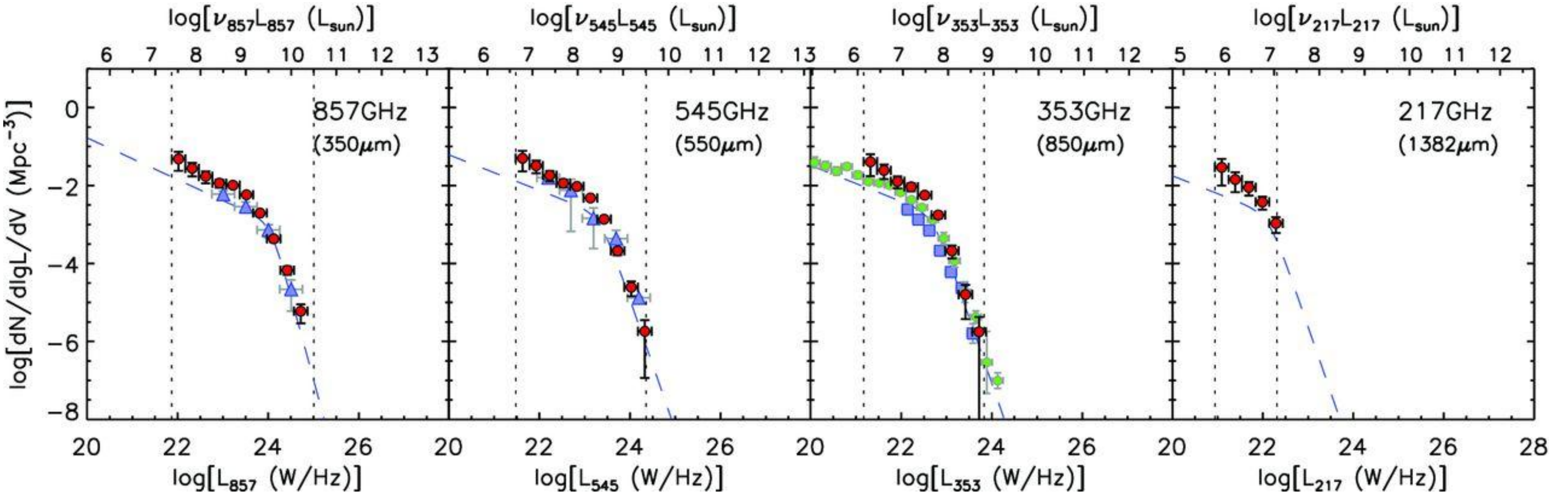

Properties of local galaxies **(Clemens et al. 2013)**

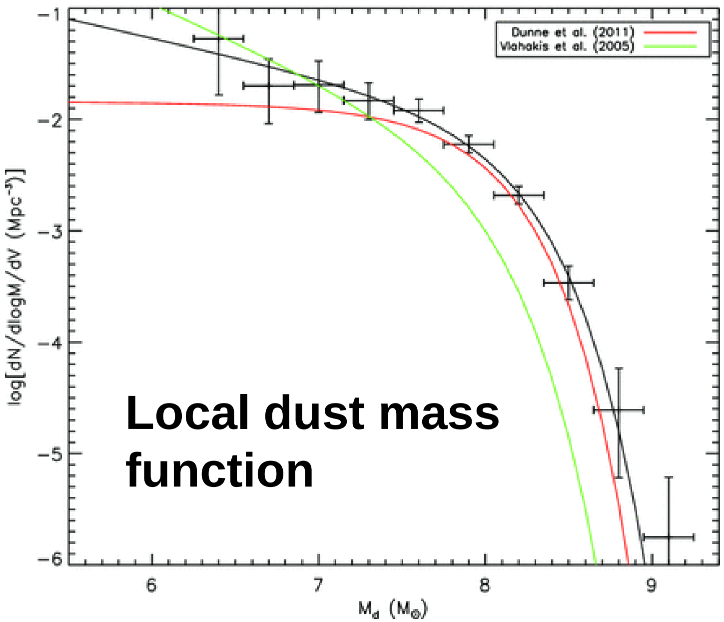

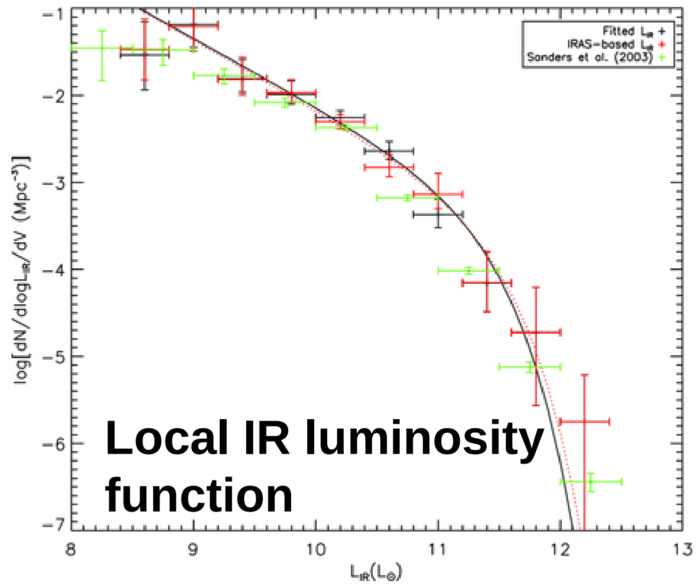

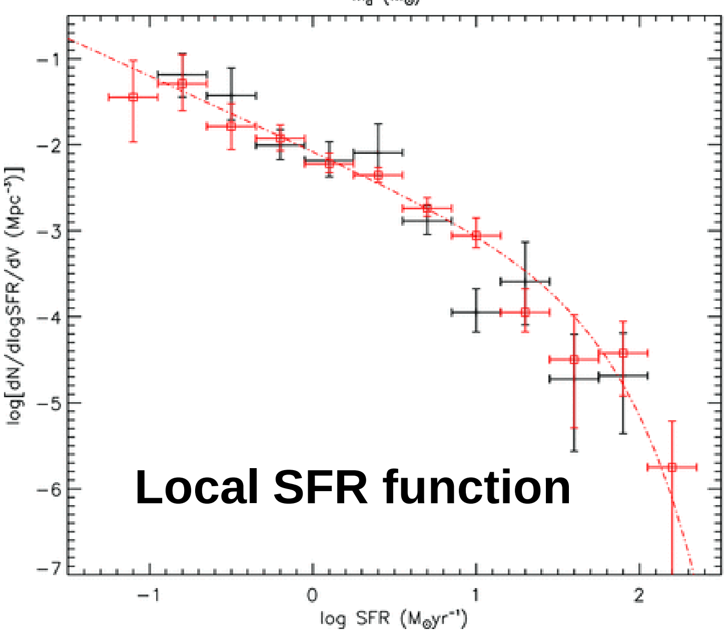

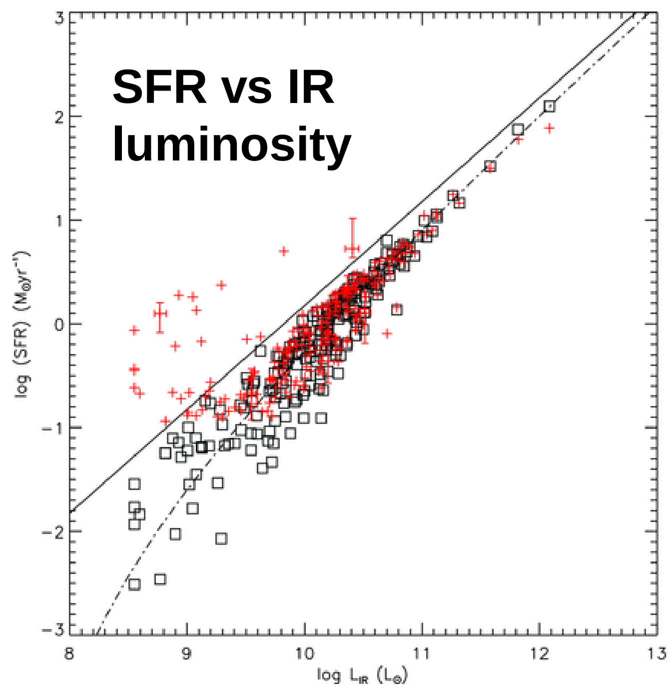

The Planck-Herschel complementarity

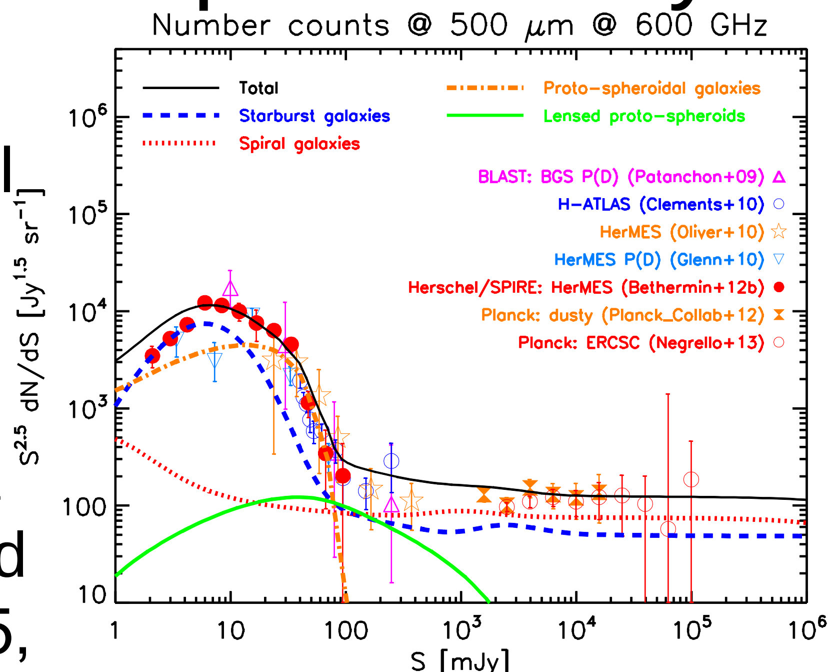

Planck extends by two orders of magnitude in flux density the Herschel counts providing corroborating evidence for the abrupt steepening of the counts at S~100 mJy which indicates the sudden appearance of a different source population, interpreted as proto-spheroidal galaxies at z ≥ 1.5, in the process of forming most of their stars. The lower-z counterparts of these sources are mostly in passive evolution and therefore minor contributors to the sub-mm counts. This abrupt steepening is very hard to account for by models interpreting the counts in terms of evolution of local populations. A sharp discontinuity in the redshift distribution of galaxies above and below ~100 mJy is confirmed by spectroscopy of strongly lensed galaxies (green line) that sample the steep portion of the counts.

Detection limits in CMB maps - 3

The variance of a Poisson distribution of sources weaker that the detection limit S_d, within a solid angle $\omega_{\rm eff}$ is

$$\sigma_P^2 = \omega_{\rm eff} \int_0^{S_d} \frac{dN}{dS} S^2 \, dS,$$

where dN/dS are the differential number counts per sr and, in the case of a Gaussian response function in polar coordinates with standard deviation θ_b ($\mathrm{FWHM} = 2\sqrt{2 \ln 2}\theta_b \simeq 2.355\theta_b$),

$$f(\theta, \phi) = \exp\left[-\frac{1}{2} \left(\frac{\theta}{\theta_b} \right)^2 \right] ,$$

$$\begin{aligned} \omega_{\rm eff} &= 2\pi \int_0^{\infty} \mathrm{d}\theta \, \theta \, f^2(\theta, \phi) = \exp\left[- \left(\frac{\theta}{\theta_b} \right)^2 \right] \\ &= \pi\theta_b^2 = \frac{\pi}{2 \, \ln(2)} \left(\frac{\mathrm{FWHM}}{2} \right)^2 . \end{aligned}$$

Detection limits in CMB maps - 4

The rms fluctuations can also be computed from the power spectrum as

$$\sigma^2 = \omega^2 \sum_\ell \frac{2\ell+1}{4\pi} b_\ell^2 C_\ell \simeq \frac{\omega^2}{2\pi} \int_0^\infty d\ell\, \ell\, b_\ell^2 C_\ell,$$

where b_ℓ is the experimental beam function, which for a Gaussian beam is well approximated by (Tegmark 1997)

$$b_\ell = \exp[-\frac{1}{2}\theta_b^2 \ell(\ell+1)],$$

and

$$\omega = 2\pi \int_0^\infty \mathrm{d}\theta\, \theta\, \exp\left[-\frac{1}{2}\left(\frac{\theta}{\theta_b}\right)^2\right] = 2\pi\theta_b^2 = \frac{\pi}{\ln(2)} \left(\frac{\mathrm{FWHM}}{2}\right)^2.$$

Note that $\omega = \omega_{\mathrm{eff}}/2$, in the Gaussian case. The approximation of the sum with the integral approximation to the sum holds if $\theta_b \ll 1\,\mathrm{rad}$ (so that the relevant $\ell \gg 1$), as is generally the case.

Detection limits in CMB maps - 5

The Poisson contribution to the power spectrum is scale-independent[a]

$$C_{\ell,P} = \int_0^{S_d} \frac{dN}{dS} S^2 \, dS \, ,$$

(Tegmark 1997). The previous expression for the Poisson rms fluctuations is then easily recovered:

$$\sigma_P^2 \simeq \frac{\omega^2}{2\pi} \frac{\pi C_\ell}{\omega} = \frac{\omega}{2} C_\ell = \omega_{\rm eff} C_\ell .$$

The spatial correlation function of galaxies, in the range of interest here, is well described by a power law, $\xi(r) \propto r^{-\gamma}$ so that the autocorrelation function of the brightness of the Cosmic Infrared Background (CIB) is $C(\theta) \propto \theta^{1-\gamma}$.

---

[a]This is because Poisson fluctuations are uncorrelated. Hence the only non-zero term of the correlation function is the one at zero-lag. Hence the power spectrum, which is the Fourier transform of the correlation function is independent of ℓ.

Detection limits in CMB maps - 6

The power spectrum of CIB intensity fluctuations due to clustering is

$$C_{\ell,\mathrm{cl}} \propto \int \mathrm{d}\theta\, \theta\, C(\theta)\, J_0(\ell\theta) \propto \ell^{-(3-\gamma)},$$

where J_0 is the Bessel function of zero order. Fits of the observed CIB power spectra yield $\beta \equiv 3 - \gamma \simeq 1.3$–$1.4$, whence

$$\sigma^2_{\mathrm{cl}} \simeq \frac{\omega^2}{2\pi} \int_0^\infty d\ell\, \ell\, b_\ell^2 C_\ell \propto \omega^\beta .$$

Thus Poisson fluctuations ($\sigma_P \propto \omega^{1/2}$) dominate on small scales while clustering fluctuations ($\sigma_{\mathrm{cl}} \propto \omega^{\beta/2}$ with $\beta/2 \simeq 0.65$–0.7) take over on larger scales.

CIB power spectra

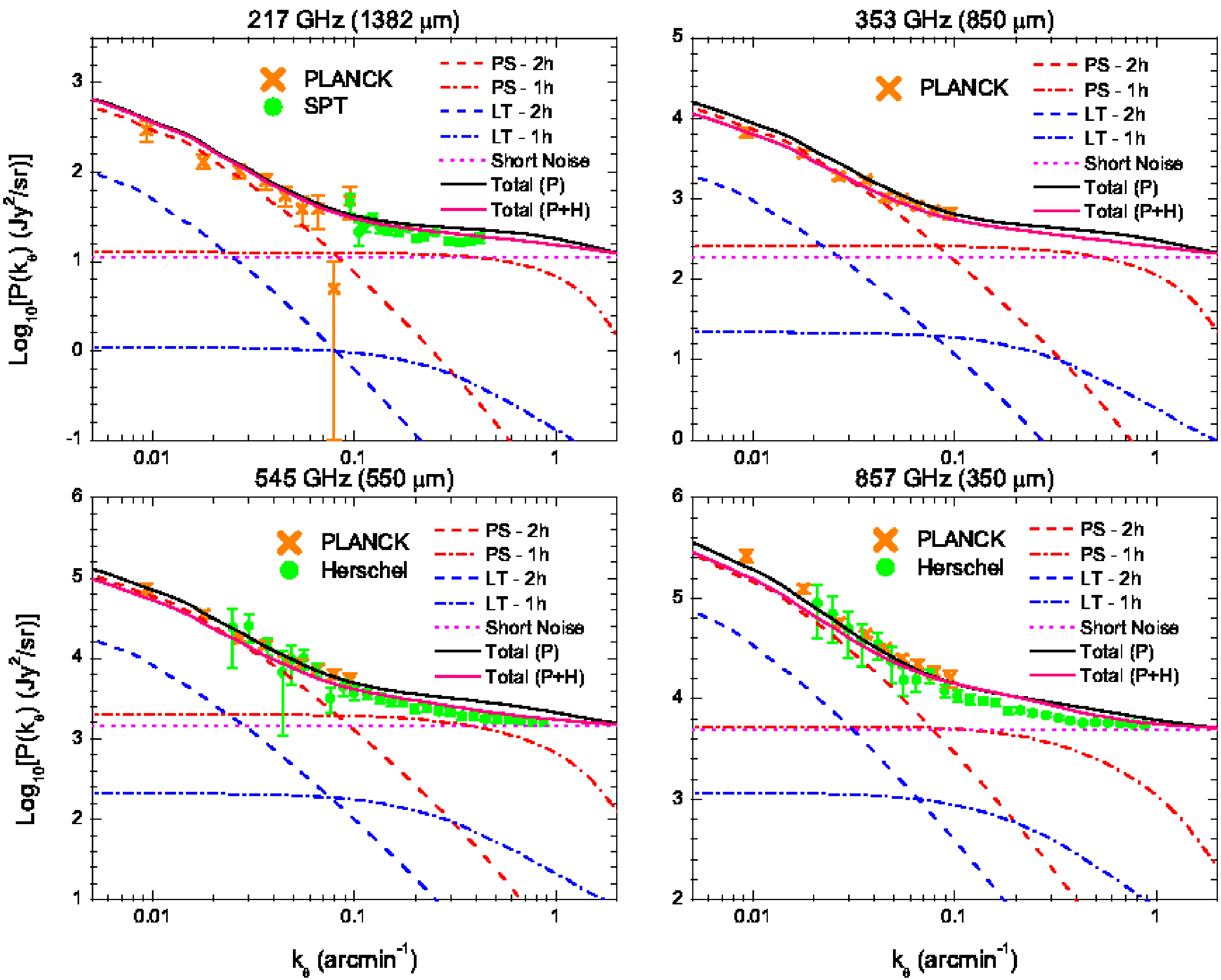

Cai et al. (2013). Data fromPlanck 2013 results. XXX and Viero et al. (2013). k (arcmin^{-1}) $= l/(2 \times 180 \times 60)$.

What can we learn from the CIB power spectrum? - 1

Under the Limber approximation, valid for the scales of interest here, the angular power spectrum at the frequency ν and at a multipole ℓ writes (e.g., Knox et al. 2001)

$$C_\ell^\nu = \int dz \left(\frac{\mathrm{d}r}{\mathrm{d}z}\right)\left(\frac{a}{r}\right)^2 \bar{j}_\nu^2(z) P_{\rm gg}(k=\ell/r, z)\,,$$

where r is the coordinate distance to redshift z, $a = (1+z)^{-1}$ is the scale factor and $\bar{j}_\nu(z)$ is the mean emissivity per comoving unit volume at frequency ν and redshift z:

$$\bar{j}_\nu(z) = (1+z)\int_0^{S_{\rm cut}} dS\; S\; \frac{d^2N}{dSdz}\,.$$

What can we learn from the CIB power spectrum? - 2

On scales large enough to be in the linear evolution phase, the power spectrum of the galaxy distribution, $P_{\mathrm{gg}}(k,z)$, writes

$$P_{\mathrm{gg}}(k,z) = b_{\mathrm{lin}}^2 P_{\mathrm{lin}}(k,z)\,,$$

where $b_{\mathrm{lin}}(k,z)$ is the redshift- and scale-dependent bias factor and $P_{\mathrm{lin}}(k,z)$ is the linear theory, dark-matter power spectrum. A more complete description of the connection between the distribution of galaxies and that of dark matter halos is provided by the halo occupation distribution (HOD) model (e.g., Berlind & Weinberg 2002; Cooray & Sheth 2002) that takes into account also non-linear structures.

Thus measurements of the CIB power spectrum provides information on the evolution of both the mean IR volume emissivity, $\bar{j}_\nu(z)$, of star-forming galaxies (hence on the evolution of the cosmic SFR) and of the bias factor (hence on the evolution of cosmic structures).

Evolution of the bias factor

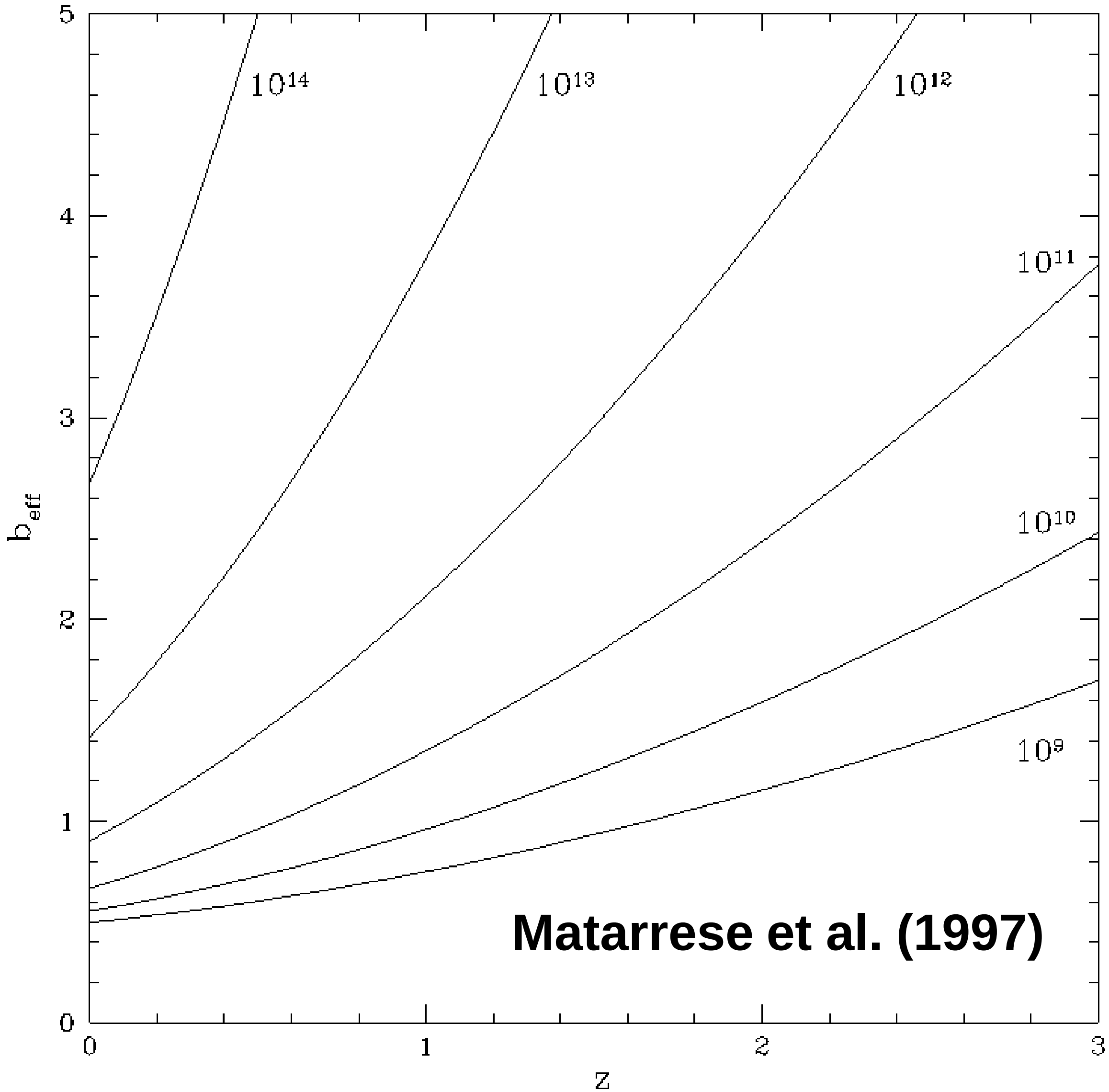

Evolution of the effective bias factor for several values of the halo mass. The amplitude of the 2-h term of the clustering power spectrum goes as b_{eff}^2 and is therefore a measure of the effective halo mass of galaxies responsible for the CIB.

What can we learn from the CIB power spectrum?

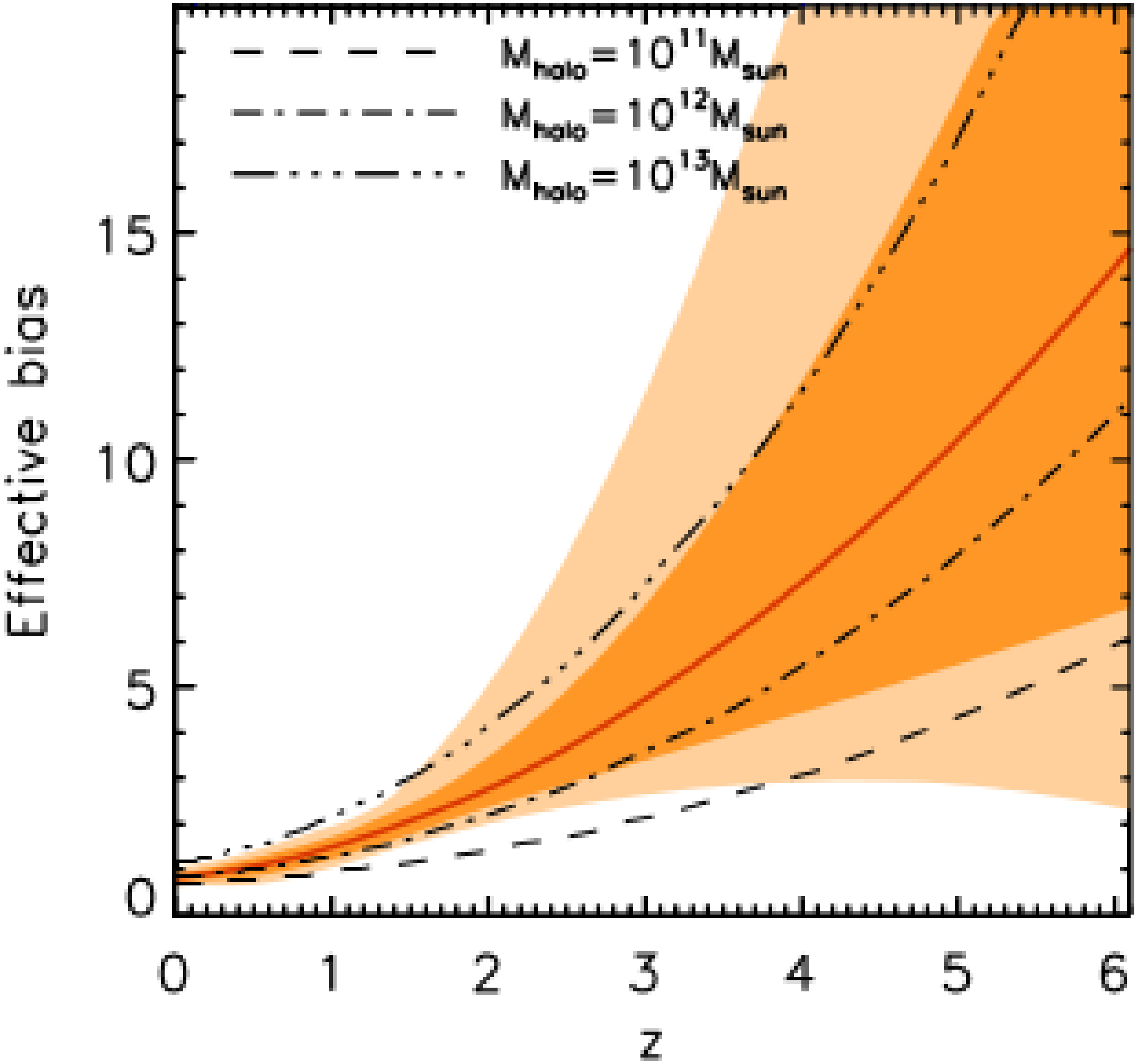

Evolution of the and effective as constrained by the linear part of the clustering power spectra. The median realization is represented by the red line, the 1σ confidence region with a dark orange area, and the 2σ region with a light orange area. From Planck 2013 results. XXX

What can we learn from the CIB power spectrum? - 3

- Estimates of the `effective' halo mass which is most efficient at hosting star formation range from $\log(M_{min}/M_{sun})$ = 12.1 to 12.7 (Xia et al. 2011; Shang et al. 2012; Viero et al. 2013; Cai et al. 2013; Planck 2013 results. XXX), close to some estimates from different observations (e.g.Tacconi et al. 2008) but somewhat higher than other estimates, based on independent data and simulations (e.g., Behroozi et al. 2012; Béthermin et al. 2012b; Wang et al. 2013).
- A somewhat puzzling result, confirmed by independent analyses, is the implied presence of a substantial non-linear contributions at $z \geq 1$ on angular scales ≥10', corresponding to physical linear scales ≥ 5 Mpc, corresponding to mass scales ≥ several $\times 10^{13} M_{sun}$ to be compared with characteristic non linear masses of $\leq 2\times10^{11} M_{sun}$

What can we learn from CIB maps? - 1

- At variance with CMB, whose fluctuations have a Gaussian distribution, the CIB anisotropies are highly non-Gaussian. This means that CIB maps contain a lot of information, beyond that contained in the power spectrum.
- The fluctuation statistics is strongly skewed in the positive side, i.e. has far more peaks with, e.g., $S/N \geq 3$ than in the Gaussian case.
- Instrumental noise is a minor contributor to fluctuations in high sensitivity experiments, like Planck.

Distribution of CIB intensity peaks at 545 GHz

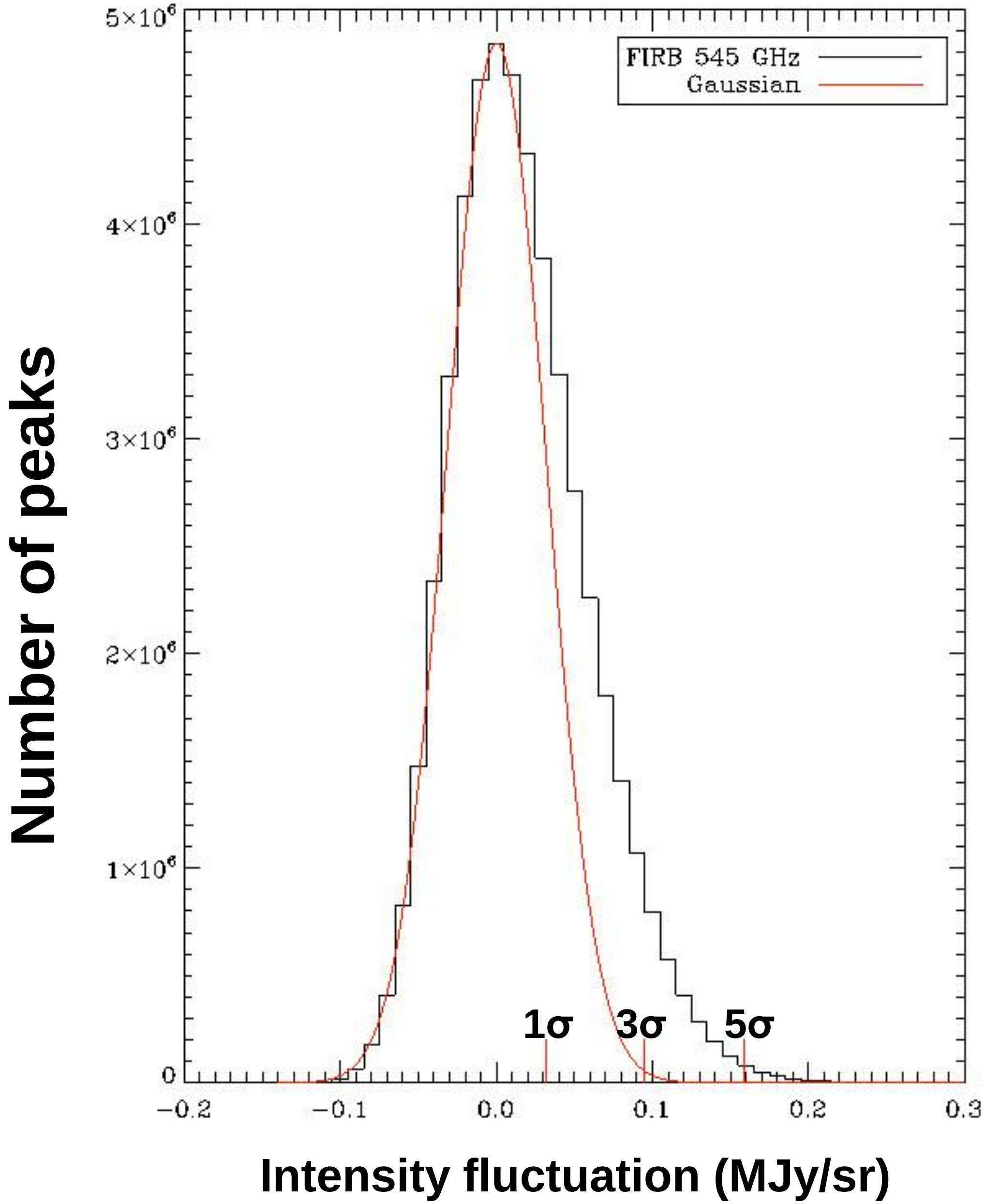

Based on the Planck Sky Model (Delabroulle et al. 2013)

Courtesy of G. Castex

What can we learn from CIB maps? - 2

- A large fraction of intensity peaks not associated to individual bright galaxies at low z may be contributed by clumps of Galactic interstellar dust (cirrus; Herranz et al. 2013) or to flat-spectrum radio sources (blazars) but others may be associated to extreme high-z sources powered by intense star-formation activity.
- Two classes of high-z non-radio sources have been detected: strongly lensed dusty galaxies and candidate proto-clusters of dusty galaxies.

Strongly lensed galaxies detected by Planck -1

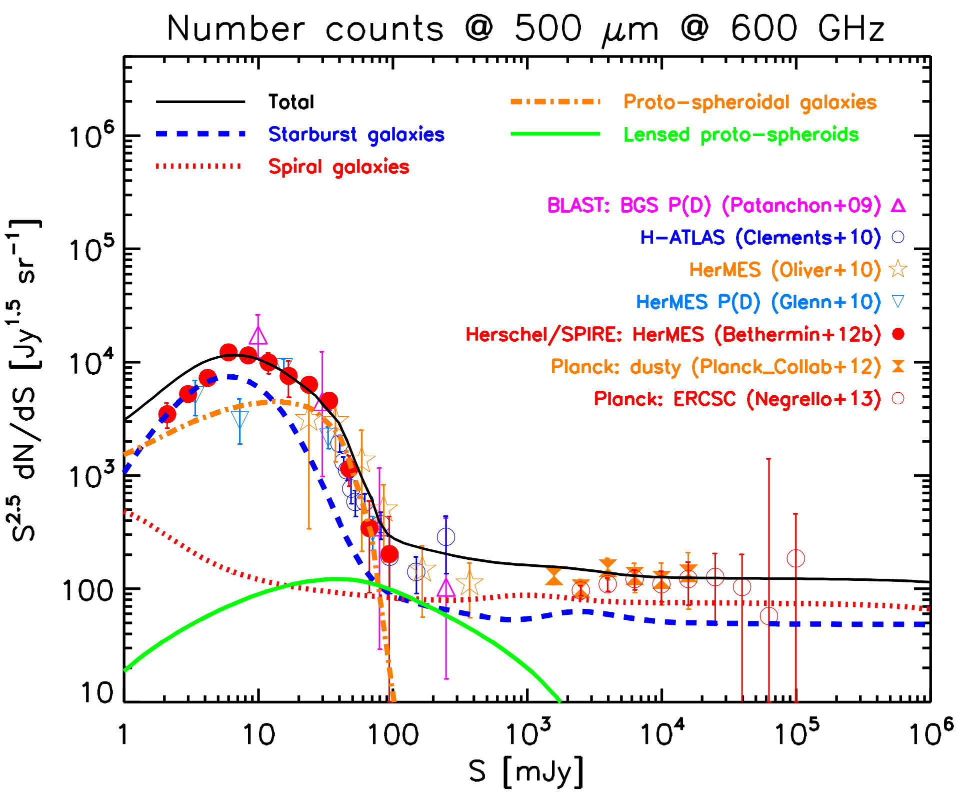

Courtesy of Zhen-Yi Cai

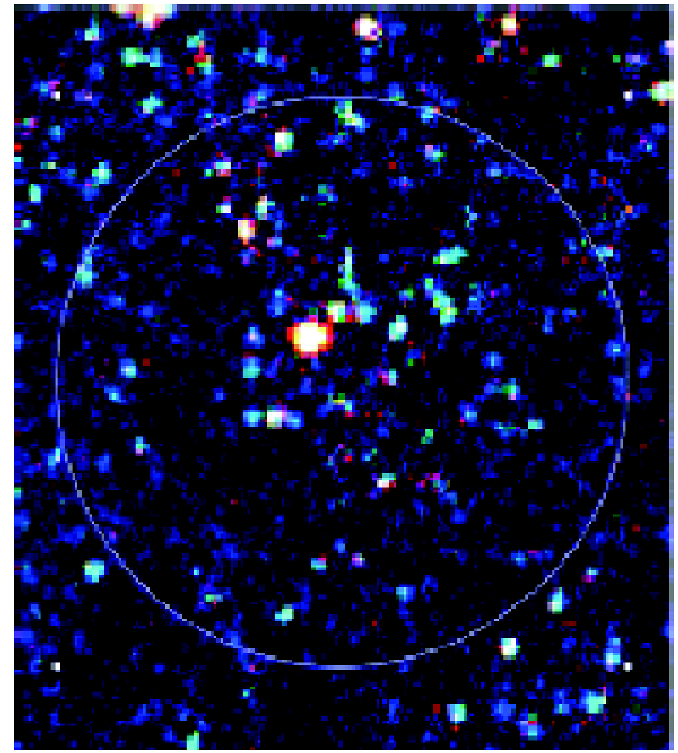

Herranz et al. (2013)

The detection limits of the Planck ERCSC are not far from the flux density range where strongly lensed galaxies are expected to show up. A boost by an underlying fluctuation peak may however make them visible (Herranz et al. z=3.26 galaxy whose Herschel flux density is ~1/3 of that measured by Planck).

Planck vs Herschel beams

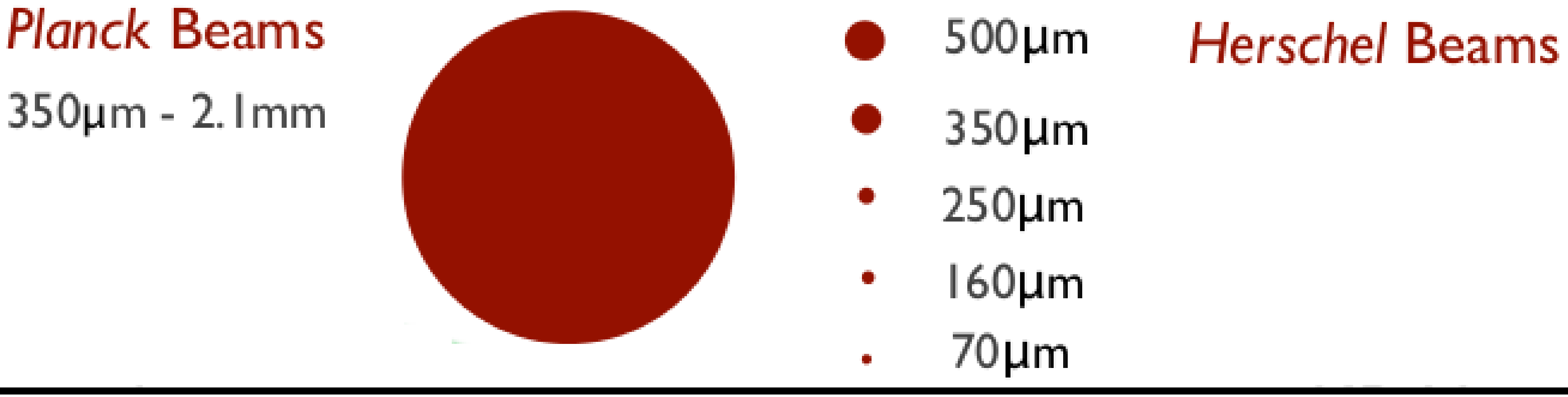

Strongly lensed galaxies detected by Planck - 2

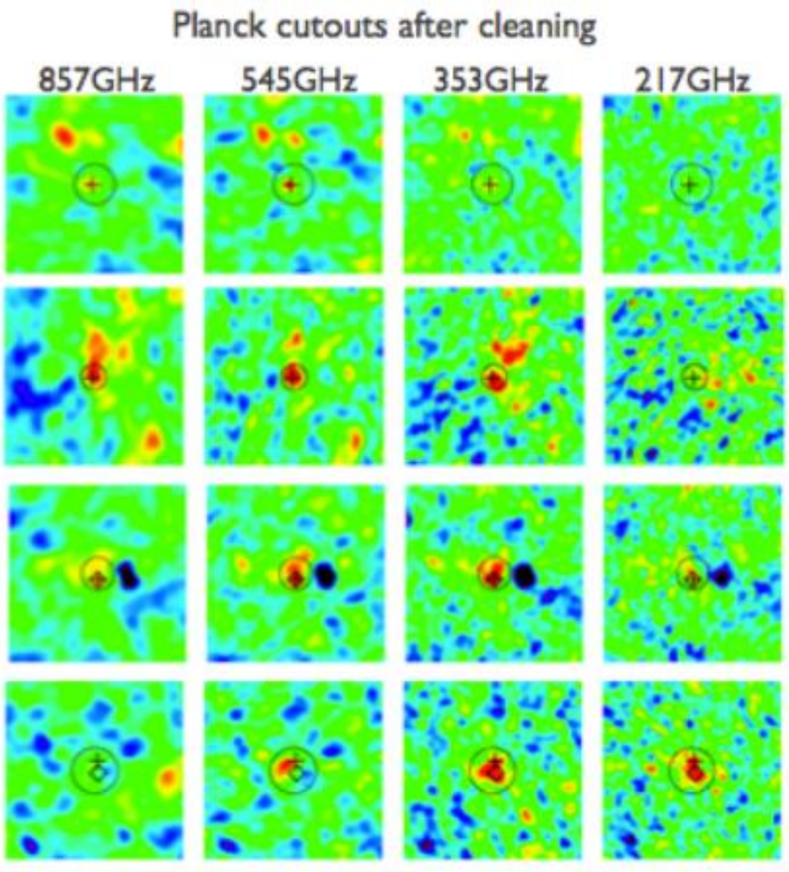

Confirmation	Redshift	Nature
SPT (1)	2.783	Lensed Dusty Galaxy (Greve et al. 2012) (Marrone et al. in prep)
Herschel ATLAS	3.26	Lensed Dusty Galaxy (Herranz et al.2012) (Fu et al. 2012)
SPT (2)	2.738	Lensed Dusty Galaxy behind a Galaxy Cluster (Greve et al. 2012) (Vieira et al. in prep)
Herschel Lensing Survey	5.2	Lensed Dusty Galaxy behind a Galaxy Cluster (Combes et al. 2012)

Herschel follow-up of Planck high-z candidates - 1

- best 35% of the sky
- several hundred Planck high-z candidates
- PCCS sources (a la Negrello+2010)
- or CIB fluctuations (a la Montier+2010)
- color-color selection

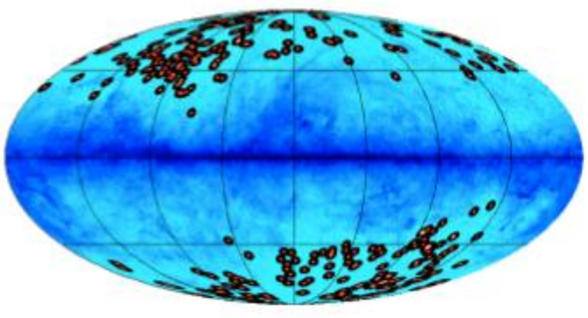

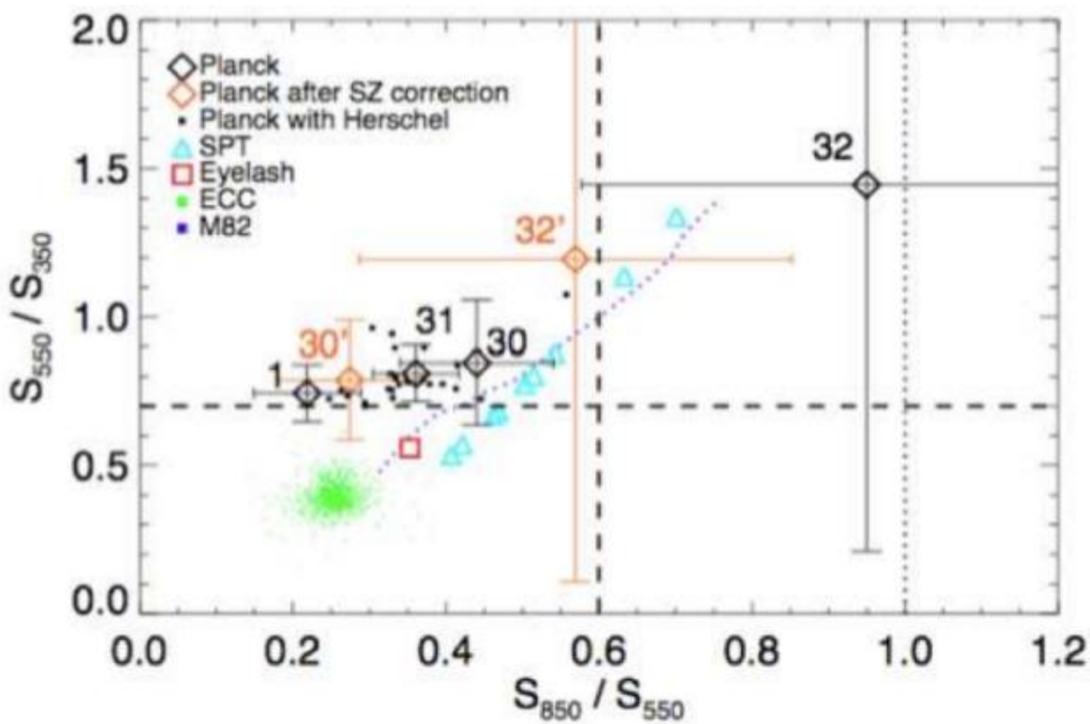

Herschel follow-up of Planck high-z candidates - 2

226 Planck sources followed-up by Herschel/SPIRE (OT1, OT2, must-do).

- **OT-1: PI Montier**
- **OT-2: PI Dole**
- **Must-Do HPASS PI Dole**

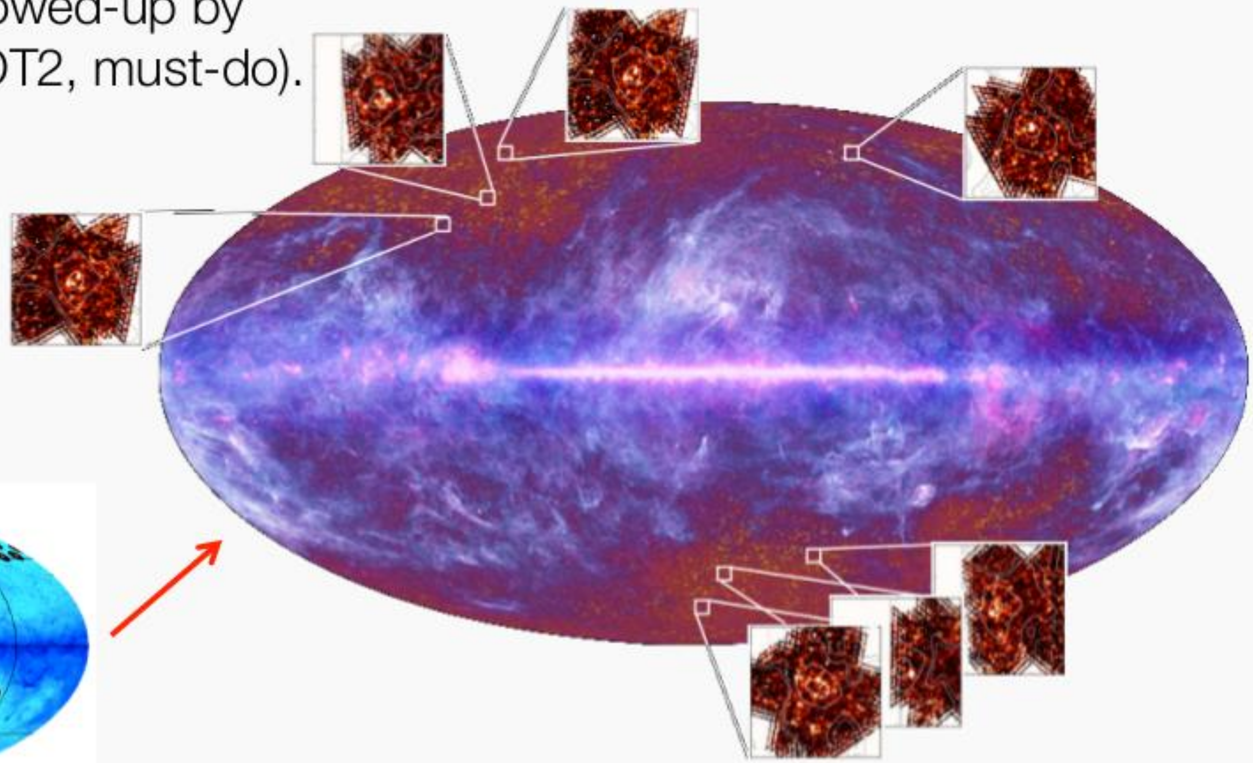

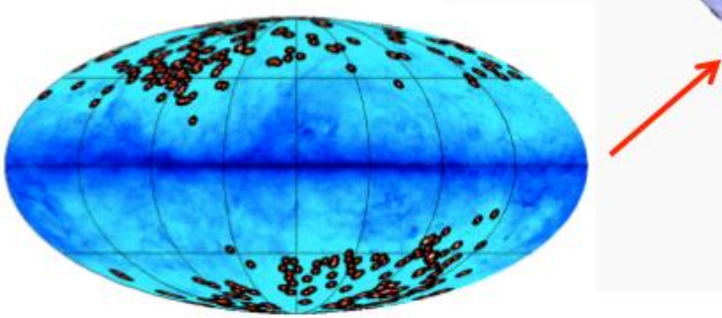

98% success
- either bright lensed candidates
- or overdensities of red galaxies
- 1.4% of the fields were cirrus

A bright strongly lensed system

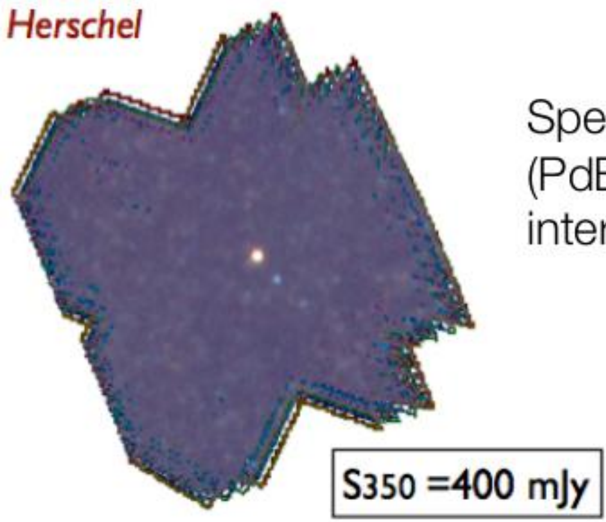

Spectroscopic data (PdBI) CO(3-2) interferometery → z = 2.59

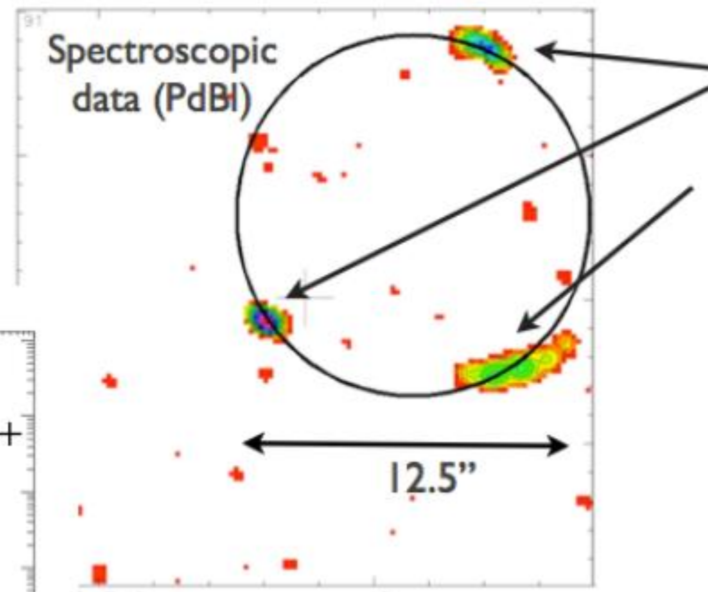

2 images of interacting galaxies

2 merging images of other or same galaxies

Highly magnified (>>10)

Waiting for lens model

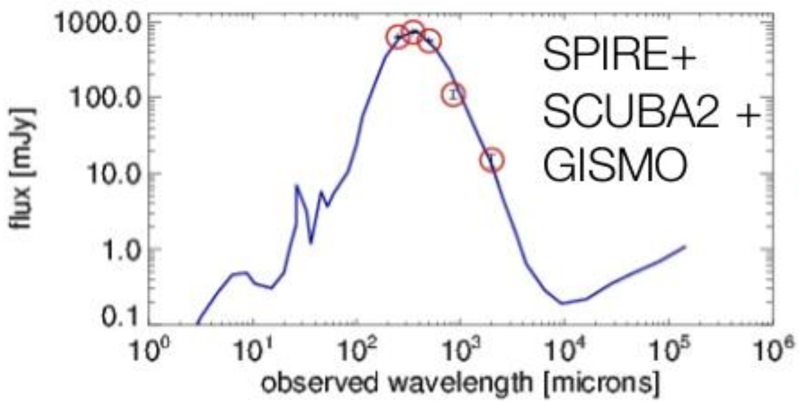

Canameras et al., in prep
Nesvadba et al., in prep

Planck detects the most luminous strongly lensed galaxies!

Looking for proto-clusters in the sub-mm - 1

- Sub-mm surveys proved to be most efficient in detecting high-z massive galaxies, interpreted as progenitors of present day giant ellipticals, caught during their star-formation phase
- There are evidences of strong clustering of these sources, consistent with them being tracers of strongly overdense regions, that will evolve into rich clusters of galaxies.
- Sub-mm surveys are therefore optimally suited to look for proto-clusters at earlier redshift than can be reached by optical/near-IR, X-ray, SZ surveys.

Looking for proto-clusters in the sub-mm - 2

- Unbiased searches of high-z protoclusters thus become possible, overcoming the need of targeting possible signposts of high density peaks (high-z radiogalaxies or powerful QSOs), as done so far.
- Low resolution instruments, like Planck, measure the sum of fluxes of sources within the beam
- The Planck all-sky survey can pick up the rare, most extreme intensity peaks.
- Within the standard gravitational clustering scenario, we expect that the distribution of intensity peaks has a very large variance, resulting from three contributions (Negrello et al. 2005).

Contributions to the variance

1. Variance of the luminosity of the most luminous source, acting as a beacon signalling the presence of the proto-cluster. This variance can be strongly enhanced by gravitational lensing.
2. Variance due to the sampling of the galaxy luminosity function.
3. Variance of the number of neighbours within the beam. Strongly dependent on the poorly known amplitude of the 3-point correlation function and on its cosmological evolution. Expected to be large.

Moments of counts of neighbours (Peebles 1980) 1

For a survey with a Gaussian angular response function:

$$f(\theta) = e^{-(\theta/\Theta)^2/2}, \quad \Theta = \frac{\mathrm{FWHM}}{2\sqrt{2\ln 2}}$$

and $\xi(r) = (r_0/r)^{1.8}$:

$$nJ_2 = n\int_V \xi(r)\, f(\theta)\, dV \simeq 25.9n\, r_0^{1.8}\, \left[D_A(z)\Theta\right]^{1.2}$$

where D_A is the angular diameter distance and:

$$\xi(r,z) = b^2(M_{\mathrm{eff}}, z)\, \xi_{\mathrm{DM}}(r,z)$$

$b(M_{\mathrm{eff}}, z) =$ bias factor, $M_{\mathrm{eff}} =$ effective halo mass,
$\xi_{\mathrm{DM}}(r,z) =$ spatial correlation function of dark matter halos.

Moments of counts of neighbours

Mean number of objects inside a volume V centered on a source:

$$\langle N \rangle_p = n \int_V [1 + \xi(r)]\, dV,$$

where n is the mean source number density. The variance around $\langle N \rangle_p$ is:

$$\langle (N - \langle N \rangle_p)^2 \rangle_p = \langle N \rangle_p + n^2 \int_V \int_V [\zeta(r_1, r_2) + \xi(r_{12}) - \xi(r_1)\xi(r_2)]\, dV_1\, dV_2$$

with

$$\zeta(r_1, r_2) = Q\,[\xi(r_1)\xi(r_2) + \xi(r_1)\xi(r_{21}) + \xi(r_{12})\xi(r_2)]\,.$$

Moments of clump luminosities

Mean luminosity of the "clump":

$$\bar{L}_{\rm cl}(z) = L_m(z) + \int_L dL'\, L'\, \Phi(L', z) \int_V [1 + \xi(r, z)]\, dV$$

with variance: **Variance of the luminosity of the most luminous source**

Variance of the number of neighbours

$$\sigma^2_{L_{\rm cl}} = \sigma^2_L + \int_L dL'\, L'^2\, \Phi(L', z) \int_V [1 + \xi(r, z)]\, dV$$

$$+ \left[\int dL'\, L'\, \Phi(L', z)\right]^2 \iint [\zeta(r_1, r_2) + \xi(r_{12}) - \xi(r_1)\xi(r_2)]\, dV_1\, dV_2 .$$

Variance due to the sampling of the galaxy luminosity function.

Luminosity function of clumps

Under the assumption that the statistics of the matter density distribution can be described by a log-normal function (Negrello et al. 2005), the probability distribution function of $L_{\rm cl}$ is:

$$p(L_{\rm cl}, z) = \frac{\exp\left[-\frac{1}{2}\left[\ln(L_{\rm cl}) - \mu_g(z)\right]^2 / \sigma_g^2(z)\right]}{\sqrt{2\pi}\;\sigma_g^2 L_{\rm cl}}$$

where

$$\begin{aligned}
\mu_g(z) &= \ln\left[\frac{\bar{L}^2_{\rm cl}(z)}{\sqrt{\sigma^2_{L_{\rm cl}}(z) + \bar{L}^2_{\rm cl}(z)}}\right], \\
\sigma_g(z) &= \ln\left[\frac{\sigma^2_{L_{\rm cl}}(z)}{\bar{L}^2_{\rm cl}(z)} + 1\right].
\end{aligned}$$

Planck 850micron counts (Negrello et al. 2005)

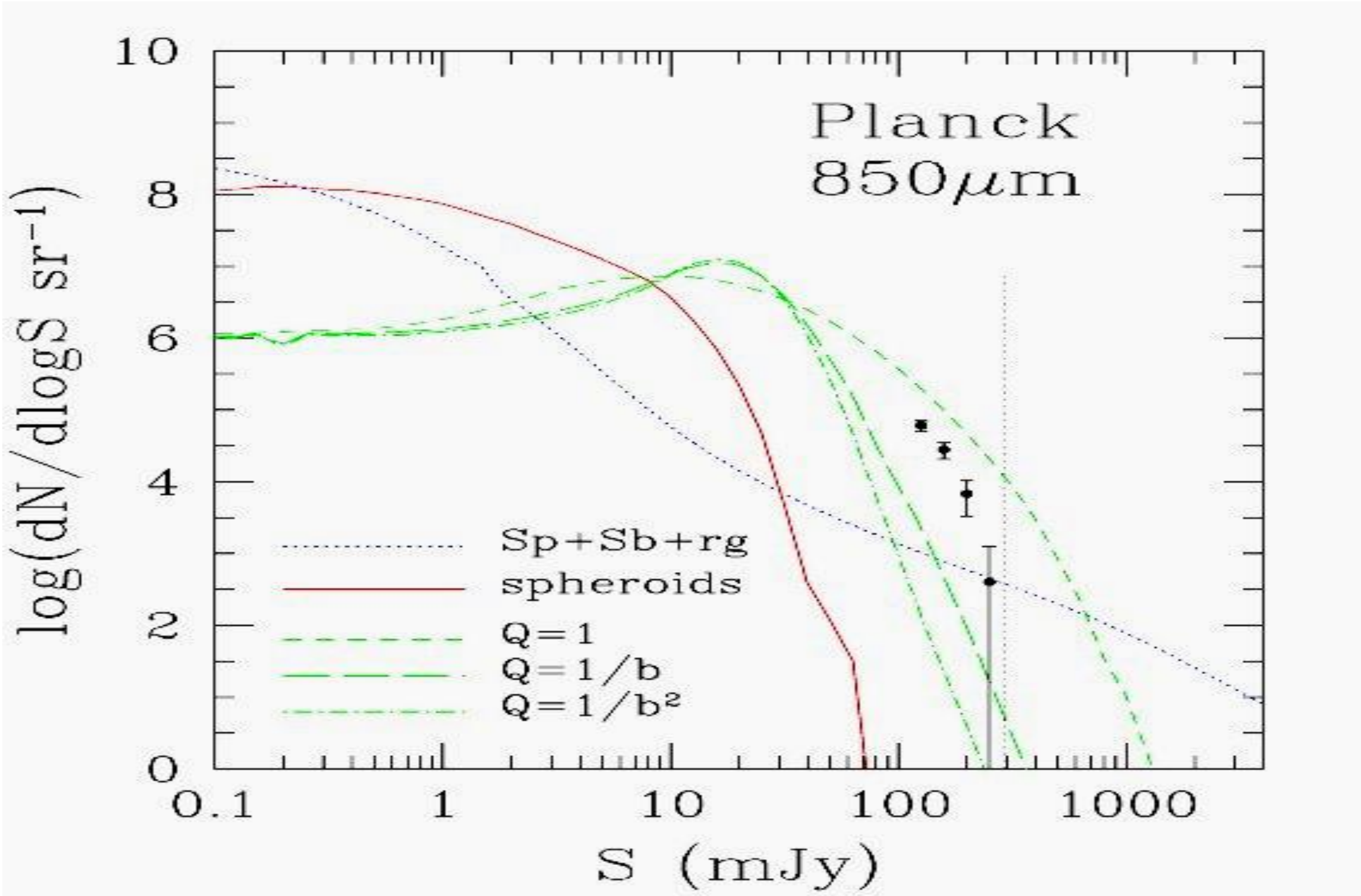

The green lines show the flux density distribution of CIB peaks due to clustering of sources whose counts are given by the magenta line for 3 evolution models for the amplitude Q of the 3-point correlation function. The points with error bars show the results of a set of numerical simulations.

Variance in the number of neighbours

Proto-clusters are located in the nodes where filaments intersect.

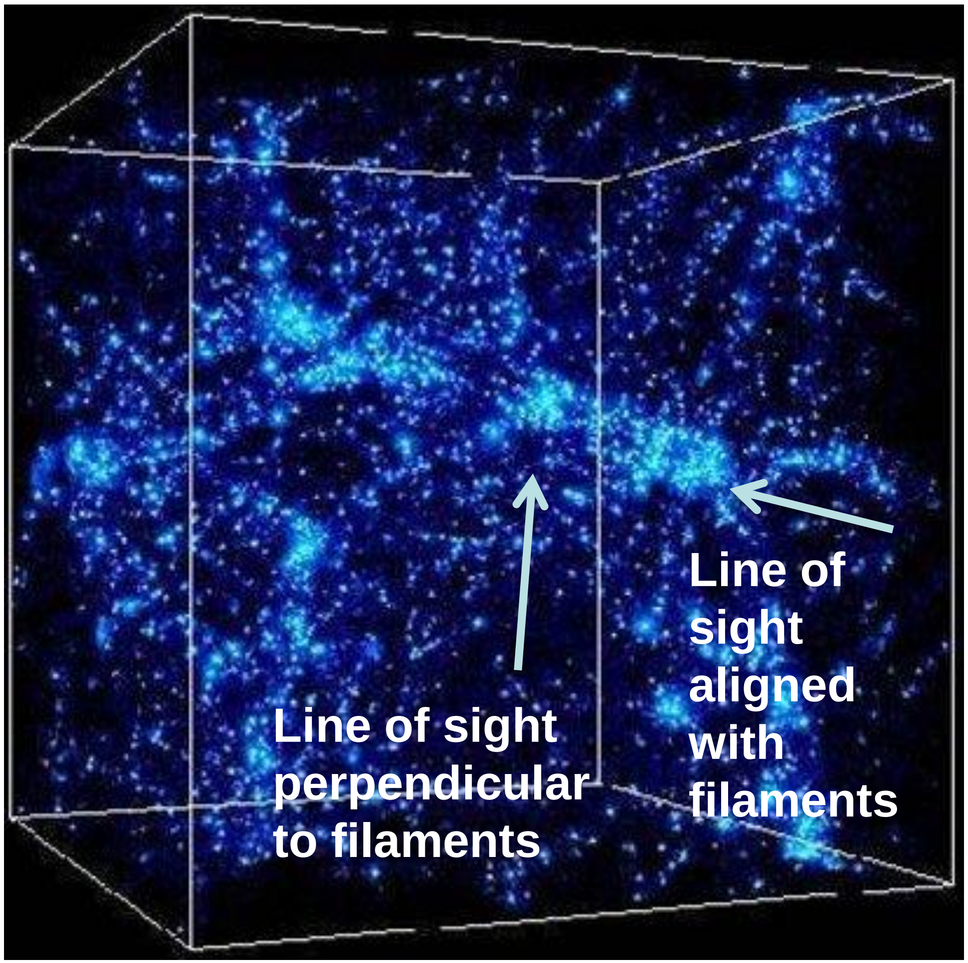

The surface density of neighbours can be widely different: compare e.g. filaments in the plane of the sky with a major filament aligned with the line of sight. Clearly, in the latter case we are not dealing with a proto-cluster.

New structure at ≥ 1.7 detected by Planck

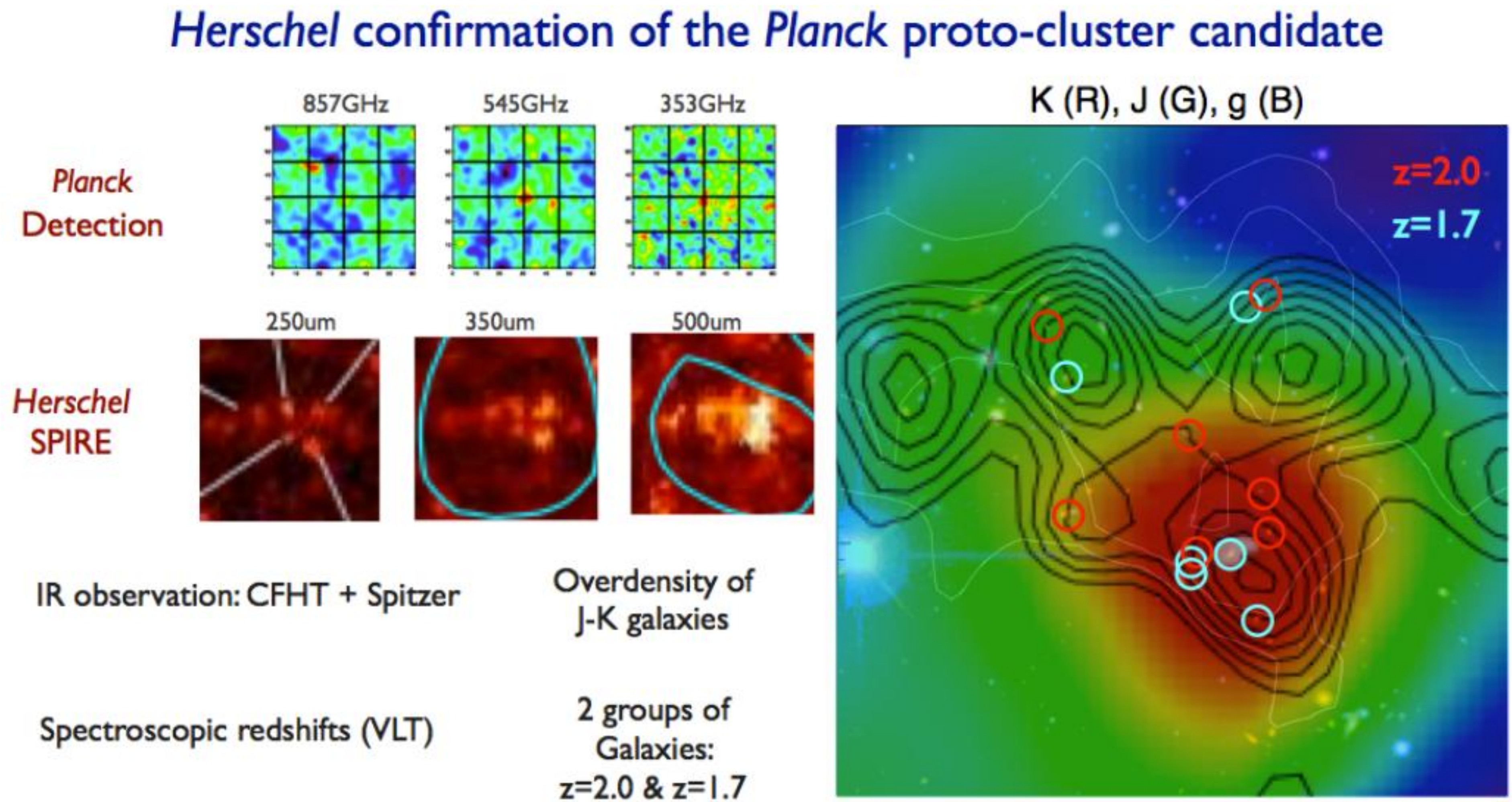

More Planck detected high-z proto-cluster candidates to be characterized by NIR and (sub)-mm imaging and spectroscopy

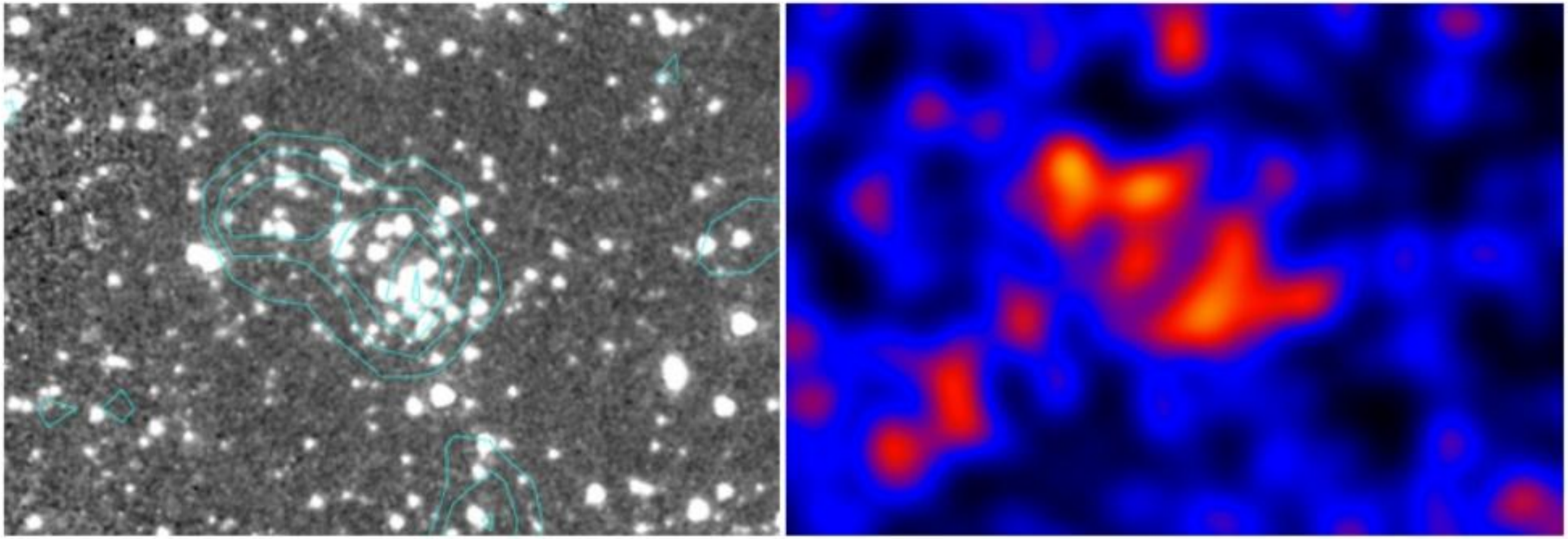

Figure 10. A high-z cluster candidate observed by *Planck*, Herschel, and here Spitzer-IRAC ($3.5' \times 2.3'$). Left: IRAC channel 2 ($4.5\ \mu$m) with SPIRE 350 μm contour. Right: color image of the 4.5/3.6 color ratio, showing the red color of the sources within the cluster candidate.

Planck sources in HerMES fields

- Clements et al. (2014) examining the Herschel-SPIRE images of the 16 Planck ERCSC sources in *Herschel Multitiered Extragalactic Survey* (HerMES) fields (~90 deg^2) found that 12 are associated with single bright Herschel sources while the remaining 4 are associated with overdensities of Herschel sources, making them candidate clusters of dusty, star-forming galaxies

Smoothed Herschel maps of candidate Planck proto-clusters (Clements et al. 2014)

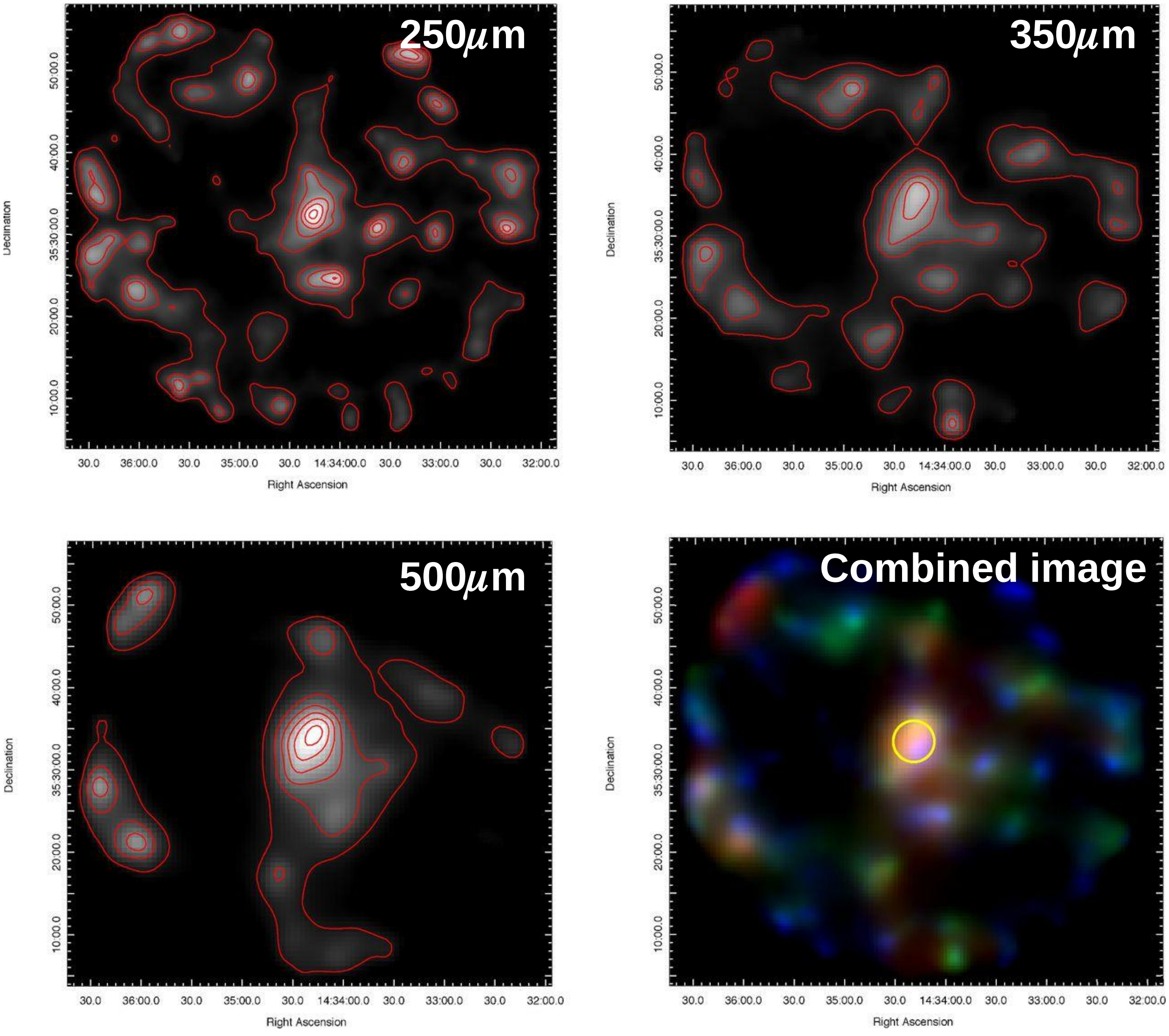

Smoothed SPIRE maps around the *Planck* proto-cluster candidate in the Bootes field at 250, 350 and 500µm (top left, top right, lower left). Lower right: colour rendition of the overdensity with blue representing 250, green 350 and red 500µm. The position of the *Planck* source position is indicated by a yellow circle representing the 4.23 arcmin Planck beam in the colour rendition.

Surface density of candidate proto-clusters compared with predictions by Negrello et al. (2005).

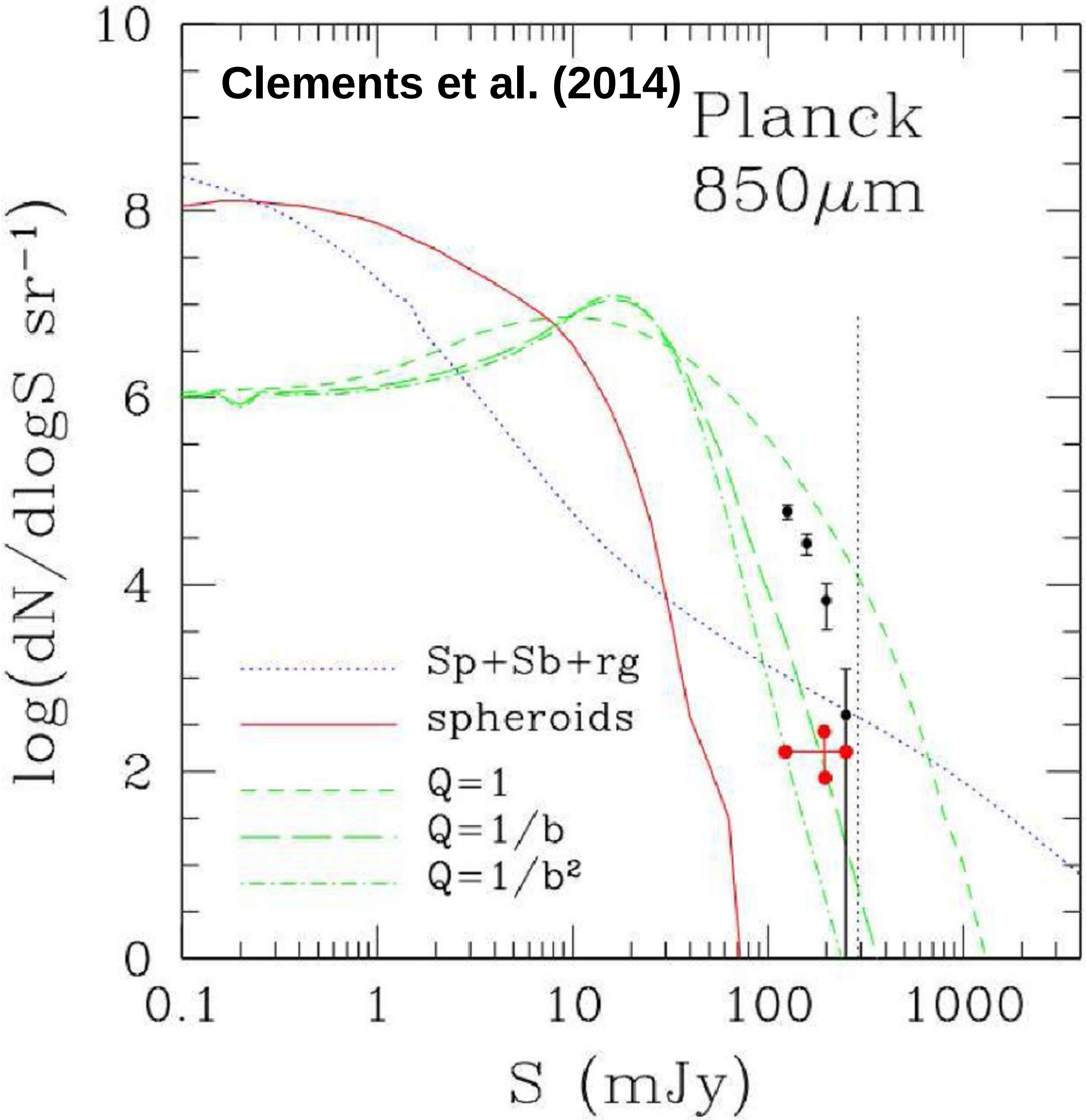

Conclusions: radio sources

- Planck is providing new insights into the SED of blazars in an essentially unexplored frequency region, close to the synchrotron peak, both directly and statistically (via source counts).
- Peak frequency uncorrelated with radio luminosity, at odds with the `blazar sequence' scenario. Results support the scenario proposed by Tucci et al. (2011)
- Some issues with sub-mm radio source counts need to be clarified

Conclusions: dusty galaxies - 1

- Planck yields the first determination of the Euclidean portion of sub-mm counts. Some models ruled out by Planck data alone.
- Substantial improvements in the estimates of the local luminosity functions at sub-mm wavelengths and first estimates at mm wavelengths.
- Accurate estimates of the statistical properties of local dusty galaxies: dust mass function, SFR function, relationship between FIR luminosity and SFR.

Conclusions: dusty galaxies - 2

- Power spectra of CIB fluctuations consistent with being dominated by galaxies with halo masses ~ $3–5\times10^{12}$ M_{sun} at z~2, independently found to be the most prolific star formers in the universe.
- Puzzling indications of non linear effects on scales ~ 10' yielded by sources thought to be at $z \geq 1$
- Red intensity peaks in Planck sub-mm maps may correspond to high-z sources: extreme strongly lensed galaxies and proto-clusters of dusty galaxies. Detection of high-z proto-clusters may be fostered if they act as gravitational lenses for background ULIRGs.